공학박사 학위논문

Functional layers of electrolyte and spectrum conversion for Dye-sensitized TiO_2 solar cells

염료감응형 TiO_2 태양전지의 전해질과 파장변환 기능층에 대한 연구

2015년 8월

서울대학교 대학원

융합과학부 나노융합전공

한 대 만

Functional layers of electrolyte and spectrum conversion for Dye-sensitized TiO_2 solar cells

지도 교수 김 연 상

이 논문을 공학박사 학위논문으로 제출함
2015 년 4 월

서울대학교 대학원
융합과학부 나노융합전공
한 대 만

한 대 만의 박사 학위논문을 인준함
2015 년 6 월

위 원 장 박 원 철 (인)

부위원장 김 연 상 (인)

위 원 송 윤 규 (인)

위 원 윤 경 훈 (인)

위 원 한 치 환 (인)

Abstract

Functional layers of electrolyte and spectrum conversion for Dye-sensitized TiO_2 solar cells

Dae-man Han
Program in Nano science and Technology
Graduate School of Convergence Science and Technology
Seoul National University

Two functional layers have been developed for enhanced stability of Dye-sensitized TiO_2 solar cells (DSSCs) : double layer gel-type electrolyte and spectrum conversion layer with 1,8-naphthalimide derivatives. In addition, a facile hierarchical microporous TiO_2 film fabrication method has been introduced for easy infiltration of quasi-solid state electrolyte.

The key element for long-term stability is the choice of sensitizing dye, electrolyte and UV cut-off filter, especially for outdoor condition. Ruthenium complex dye (N719) has been widely used due to high photo-to-current conversion efficiency and proved

stability. However, there has been contradiction between photo-to-current conversion efficiency and long-term stability in the choice of electrolyte and UV cut-off filter.

To enhance the photo-to-current conversion efficiency of long-term stable UV-cured polymer gel electrolyte, additional nano-gel electrolyte layer was introduced between the above-mentioned electrolyte and counter electrode. Resultant double layer gel-type electrolyte showed a lower charge transfer resistance due to the increase of exchange-reaction-based charge diffusion effect despite the negative influence from increase of electrolyte thickness.

A crucial factor using quasi-solid state electrolyte is decreasing contact resistance between TiO_2 nanoparticulate film and electrolyte. To accomplish easy infiltration of electrolyte into the TiO_2 nanoparticulate film, micro-crater structure was formed using acetylene-black as an evaporated material at high temperature. This morphology control improved light scattering effect without using additional light scattering layer.

Titanium dioxide nanoparticles provide the support for binding of sensitizing dye, however, in case of UV light irradiation, they act as a photocatalyst inducing the degradation of sensitizing dye and decrease of redox couple. To convert damaging UV light into useful longer wavelength light in advance, additional spectrum conversion layer

with UV absorbing 1,8-naphthalimide derivatives was introduced on the photo-anode. This functional layer absorbed effectively the UV light in advance and emitted a useful longer wavelength light by Stokes fluorescence.

In this research, three new methods were developed using Dye-sensitized TiO_2 solar cells with Ruthenium complex dye to avoid unexpected influence from environment. However, these new techniques can be applied extensively to the next generation solar cells regardless of the kind of device to improve the long-term stability while maintaining high photo-to-current conversion efficiency.

Keywords: Dye-sensitized solar cell, long-term stability, gel-type electrolyte, hierarchical TiO_2 film structure, spectrum conversion layer

Student Number: 2010-30738

Contents

List of Figures

the the two electrode glasses

Figure 18. Optical properties of the TiO_2 photo-anode films containing 1 wt.% of acetylene-black measured by spectrophotometer according to the heat treatment conditions of 200 ℃ for 60 minutes, 450 ℃ for 60 minutes, and 550 ℃ for 5 minutes. Each photograph images indicated inset correspond to each measured points.

Figure 19. Optical properties of the TiO_2 photo-anode films containing 1 wt.% of acetylene-black measured by spectrophotometer according to the heat treatment times of 5 minutes, 30 minutes, and 50 minutes at 550 ℃. Each photograph images indicated inset correspond to each measured points.

Figure 20. Comparison of the Transmittances of the TiO_2 photo-anode films prepared as bare FTO glass, normal TiO_2 film screen printed one time or three times, AB TiO_2 film screen printed one time or three times, respectively. Here, A.B. denotes the acetylene-black.

Figure 29. (a) General synthetic route and numbering (b) representative formula of 1,8-naphthalimide derivatives; Family of derivatives are synthesized by the reaction of 1,8-naphthalic anhydride (6,7-dimethoxy-benz[*de*]isoquinolin-1,3-dione) with kinds of alkyl amines. Representative formula is (2-(1-ethylhexyl)-6,7-dimethoxy-benz[*de*]isoquinolin-1,3-dione), CAS No. 139106-96-0, Molecular Formula $C_{22}N_{27}NO_4$ and Molecular Weight 369.45 g/mole

Figure 30. Transmittances of TiO_2 sol coated FTO glasses; TiO_2 sol was coated 1, 2 and 3 times on FTO glasses as a reference UV absorbing materials, corresponding to TiO_2 sol #1, #2 and #3, respectively.

Figure 31. Transmittances of FTO glasses with SCL of 0, 0.5, 1.0, 1.5, 2.0, 2.5 and 3.0 wt.% 1,8-naphthalimide derivatives, respectively.

Figure 32. Reflectances of SCL and TiO_2 sol coated FTO glasses; The concentration of 1,8-naphthalimide derivatives was

optical filter, (ii) 1,8-naphthaimide derivatives 0 and 2 wt.% as SCL and (iii) commercial UV cut-off filter, respectively.

Figure 38. Transmittance and reflectance of commercial UV cut-off filer;

Figure 39. Difference of photo-to-current conversion efficiency of DSSCs with SCL and bare DSSC. The concentration of 1,8-naphthalimide derivatives was 2 wt.%.

Figure 40. Incident Photon-to-Current conversion efficiencies (IPCE) of the prepared DSSCs using (i) bare FTO glass without any optical filter, (ii) 1,8-naphthaimide derivatives 0 and 2 wt.% as SCL and (iii) commercial UV cut-off filter, respectively.

Figure 41. Relative outdoor photo-to-current conversion efficiencies of the prepared DSSCs using (i) bare FTO glass without any optical filter, (ii) 1,8-naphthaimide derivatives 0 and 2 wt.% as SCL and (iii) commercial UV cut-off filter, respectively.

List of Tables

Chapter 1. Introduction

1.1 Research trends

Total installed capacity for solar PV globally amount to at least 177 gigawatts by the end of 2014, up from nearly 140 gigawatts in 2013. There is at least 10 times more solar PV installed around the world today than in 2008. These global installations are now producing more than 1 percent of the electricity used on the planet.

A photovoltaic cell is an electrical device that converts the energy of light directly into electricity by the photovoltaic effect. First generation PV cells are single crystalline silicon and multi-junction cell incorporating different bandgap materials. Second generation PV cells are thin film silicon, CdTe and $CuInSe_2$. Third generation PV cells are polymer cells with quantum dots or nanostructures including dye-sensitized solar cells (DSSC).

For the commercial production of DSSC, several pilot lines have been installed or are under construction. A first full production line is under operation since 2012 for flexible DSSC. Due to the beneficial low-light performance of DSSC the first attractive market for products is the consumer electronic market. A particular aspect of DSSC is the

possibility for a decentralized local production which is realized by the early stage market introduction of DSSC modules for solar home systems. The recent success in up-scaling of DSSC modules demonstrates the suitability of DSSC for the potentially very large building integrated PV market, although a certification step is still required.

Dye-sensitized solar cell is the only photovoltaic device that mimics the photosynthesis process as in plants. Artificial photosynthesis using colloidal TiO_2 electrode with derivatives of chlorophyll and related natural porphyrins have approached the unity efficiency of primary charge separation in natural photosynthesis.[1]

Dye-sensitized TiO_2 solar cells in this thesis uses TiO_2 electrode as a charge collector to separate electron from the excited state sensitizing dye to the photo-anode side. When DSSC is exposed to light, sensitizing dye absorbs photons and goes to an excited state that lies energetically above the conduction band edge of TiO_2 electrode. (**Fig.1**) Three main reactions are followed on TiO_2 electrode, i.e.[2]

(a) Electron injection from an excited state dye to conduction band of TiO_2;

(b) Hot electron injection or cooling processes of the hot electron in the conduction band and in trap states;

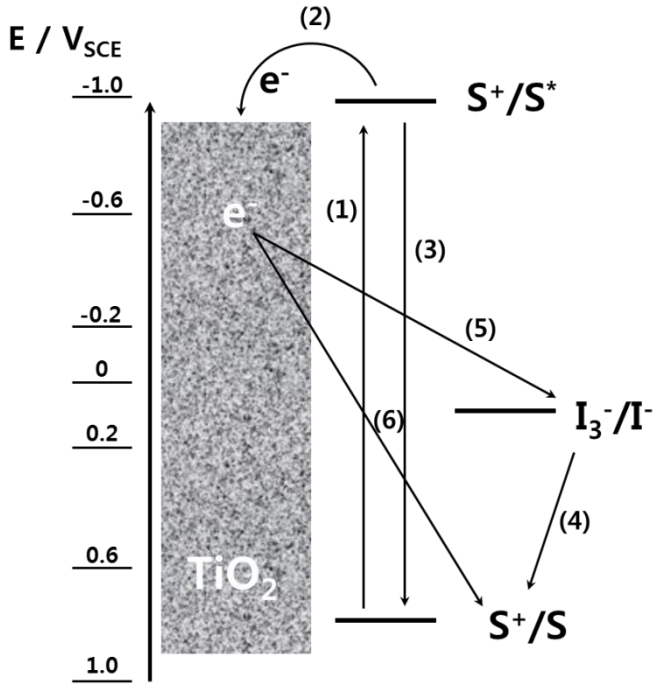

Fig. 1. Energy level diagram of Dye-sensitized TiO_2 solar cell.

(c) Recombination between conduction band of TiO_2 and dye cation and/or capture by redox couple.

The properties of sensitizers are most important for high photo-conversion efficiency in TiO_2 electrode DSSC. Required properties of sensitizers are listed in **Fig.2(a)** and light absorption spectrum of N719 dye versus solar irradiance is shown as a representative example in **Fig.2(b)**.

Sensitizing dyes have been developed from ruthenium dyes to organic dye and porphyrin dye. Photo-conversion efficiency was over 10% when Nazeeruddin *et at*. reported synthesizing ruthenium complex dyes named N3 dye and N719 dye.[3] Although, ruthenium complex dye accomplished higher photo-conversion efficiency and better stability, ruthenium complex dye was very expensive for commercialization and toxic for environment. To address these issues, there were approaches to synthesize metal-free organic dyes as coumarin dyes, polyene dyes, and indoline dyes. Tamotsu Horiuchi *et al*. reported high photo-conversion efficiency of 9.5% using metal-free indoline dyes in 2004.[4] Following metal-free organic dyes, DSSC using porphyrin dye has changed the color of solar cells from red to green with higher photo-voltage and photo-conversion efficiency.[5]

(a) Required properties of sensitizers

① Broad spectral coverage

② High absorption cross-section

③ Appropriate energies to match oxide & redox

④ Fast kinetics for injection and regeneration

⑤ Stability for many (~10^8) turnovers

(b)

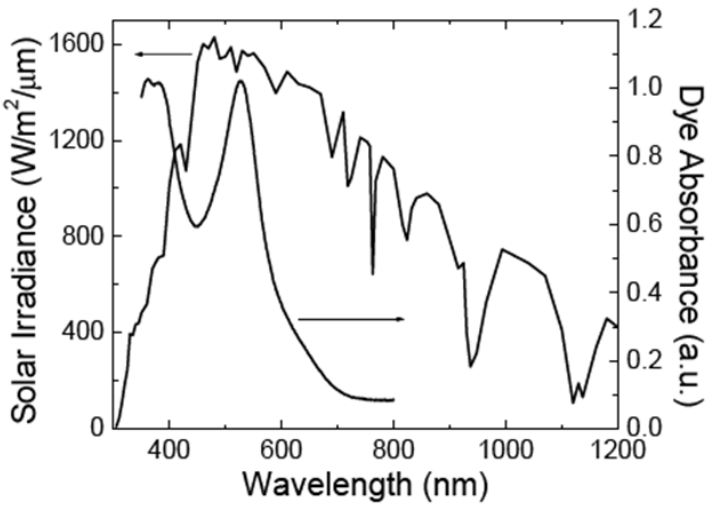

Fig. 2. (a) Required properties of sensitizers and (b) light absorption spectrum of N719 dye versus solar irradiance.

Evolution of photo-to current conversion efficiencies for DSSC is shown in **Fig.3**.[6] Recently, natural dyes and D-π-A metal-free organic dyes were introduced in correspondence to the several disadvantages of using noble metals in DSSC: noble metals are limited in amount, hence raise the production cost. However, organic dyes have shown problems as well, such as complicated synthetic routes and low yields.

Therefore, natural dyes found in flowers, leaves, and fruits are receiving much attention as a sensitizer that can be extracted by simple procedures. Huizhi Zhou *et al.* introduced 20 natural dyes as sensitizers in 2011.[7] Regardless of organic and natural dyes, previous approaches of using metal-free organic dyes were unsuccessful due to a narrow absorption band in the visible region, aggregation and poor stability of solar cells.

A major breakthrough came with the incorporation of a donor-π-acceptor (D-π-A) structure which facilitates photo-induced charge separation. This spatial orientation not only favors the electron injection, but also slows down the recombination of separated charges. Recent research on the optimization of D-π-A dyes is mainly focused on:[8]

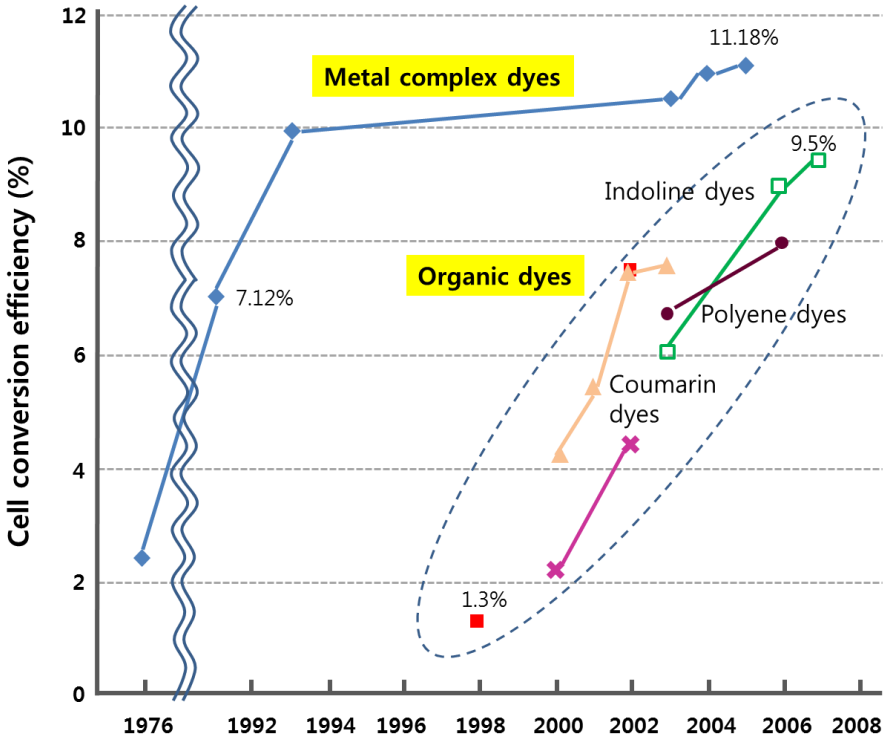

Fig. 3. Evolution of photo-to-current conversion efficiencies for DSSC.

Tuning the absorption band of the dye to achieve a better match with the solar spectrum and a broader absorption in the near-infrared region;

(a) Minimizing the energy level mismatch between the excited state dye oxidation potential and TiO_2 conduction band, and HOMO and electrolyte to avoid potential losses;

(b) Lowering the charge recombination rate at the TiO_2/electrolyte interface;

(c) Suppressing dye aggregation;

(d) Increasing the stability of DSSC based on organic dyes.

Quantum dot (QD) sensitizer is a semiconductor nanoparticle that can be applied to a free-standing ink and used for cheap spray-on solar cells, in case the performance and stability are improved in the future. Near-infrared absorbing PbS QDs are promising candidates for photovoltaic applications due to convenient energy bandgap tunability. However, Solution processing of QDs for device fabrication remains a major technical challenge to achieve high efficiency and good atmospheric stability. Chia-Hao M. Chuang *et al.* addressed this issue with room-temperature solution-processed ZnO/PbS QD solar cells. Photo-conversion efficiency of 8.55 % was reported by engineering

the band alignment of the QD layers through the use of different ligand treatments.[9] However, QD solar cells of most efficiency have been prepared with toxic heavy metals of Cd or Pb. Solar cells based on green QDs – totally free of Cd or Pb – presented only a modest photo-conversion efficiency. To improve the photo-to-current conversion efficiency of green QD solar cells, Zhenxiao Pan *et al.* reported effective surface passivation technique of the ternary $CuInS_2$ QDs that can provide high photovoltaic quality core/shell CIS/ZnS QDs, that surpass the performance of those based on the toxic cadmium and lead chalcogenides QDs.[10]

Perovskite material as another sensitizer has a crystal structure of cubic metal halide with chemical formula ABX_3. Organic or inorganic cations occupy position A, whereas metal cations and halides occupy the B and X positions, respectively. (**Fig.4**)[11] Merits of perovskite material are as follows:

(a) Light absorption coefficient is 10 times higher than commonly used N719 ruthenium dye
(b) Light absorption spectrum is up to 800 nm
(c) Charge diffusion length is very long

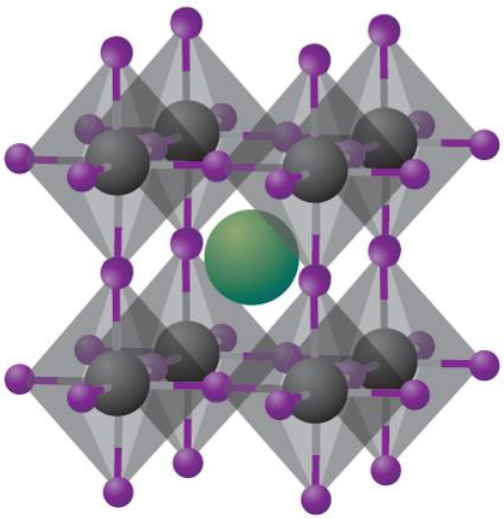

Fig. 4. Crystal structure of cubic metal halide perovskites with the chemical formula ABX_3. Organic or inorganic cations occupy position A (green) whereas metal cations and halides occupy the B (grey) and X (purple) positions, respectively.

Photo-to-current conversion efficiency of perovskite solar cell is ascending higher on the benefit of several merits listed above. Evolution of perovskite solar cell from a mesoscopic to a planar embodiment is shown in Fig.5. Figure (a) is employing a film of Al_2O_3 nanocrystals covered with a conformal overlayer of $CH_3NH_3PbI_3$ perovskite, which act as a light harvester as well as an electron conductor. Figure (b) is a nanocomposite embodiment where the mesoscopic TiO_2 scaffold is infiltrated by the perovskite, which act as a light harvester as well as a hole conductor. Figure (c) is a planar heterojunction solar cell lacking the TiO_2 mesoporous scaffold. In the field of perovskite material research, compositional engineering is a key factor for higher photo-conversion efficiency. Photo-to-current conversion efficiency of 16~17% was obtained for solution-processing method of methylammonium iodide ($MAPbI_3$). Recently, PCE of 18.4% was obtained in thick mesoporous TiO_2 layer and PCE of 20.3% was obtained in thin mesoporous TiO_2 layer through compositional engineering using formamidinium lead iodide ($FAPbI_3$) and methylammonium lead bromide ($MAPbBr_3$).[12] Field of perovskite solar cells is in a dynamic state, however, hysteresis, stability and toxicity issues remain.

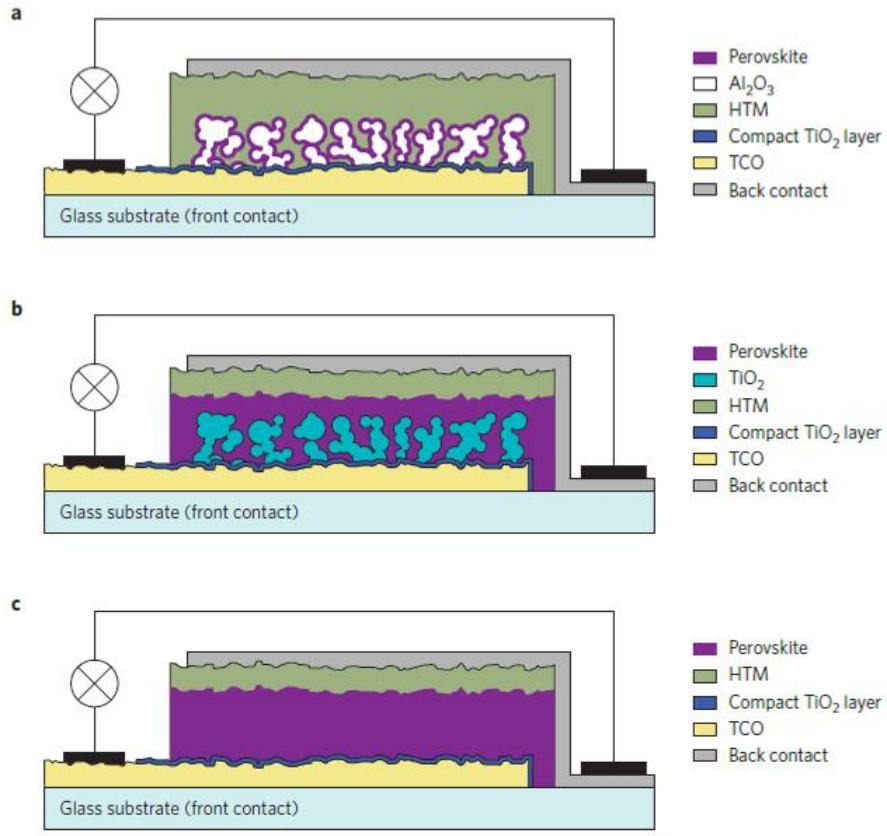

Fig. 5. Evolution from a mesoscopic to a planar embodiment of the perovskite solar cell.

1.2 Objectives of DSSC

Since, Grätzel and co-workers first reported 7.1~7.9 % in 1991,[13] dye-sensitized solar cells have received much attention as an alternative to conventional silicon-based solar cells due to their high conversion efficiency, simple fabrication process, potential for low cost production, low CO_2 consumption at production, and colorful appearance.[14] Recently reported best photo-to-current conversion efficiency was 13 %, achieved through the molecular engineering of porphyrin sensitizers.[15]

Confirmed terrestrial cell efficiency of DSSC is 11.9 %, which is lower than silicon crystalline 25.6 % or CIGS cell 20.5 %, but slightly higher than silicon amorphous 10.1 % or organic thin film 10.7 %. Notable results not measured under the global AM1.5 spectrum (1,000 W/㎡) at 25 ℃ are shown for perovskite thin film 17.9 % and organic thin film 11.1 %. (see **Table 1**) [16]

Current main sector of DSSC application is in indoor, portable and disposable electronics, but, DSSCs are forecasted to penetrate in several market segments including BIPV, PV for developing countries, wireless sensors/actuators, electronics in apparel and emergency and

Table 1. A summary of confirmed terrestrial cell efficiencies Adapted from M. A. Green *et al. Prog.Photovolt: Res. Appl.* 2014; **22**:701-710

Classification	**Efficiency (%)**	**Area**① **(㎠)**	**Description**
Silicon			
Si (crystalline)	25.6 ± 0.5	143.7 (da)	Panasonic HIT
Thin film chalcogenide			
CIGS (cell)	20.5 ± 0.6	0.9882 (ap)	Solibro, on glass
Amorphous Si			
Si (amorphous)	10.1 ± 0.3	1.036 (ap)	Oerlikon Solar Lab, Neuchatel
Dye sensitised			
Dye sensitised	11.9 ± 0.4②	1.005 (da)	Sharp
Dey (submodule)	8.8 ± 0.3[b]	398.8 (da)	Sharp
Organic			
Organic thin film	10.7 ± 0.3③	1.013 (da)	Mitsubishi Chemical
Organic (submodule)	6.8 ± 0.2[c]	395.9 (da)	Toshiba
Notable Exceptions			
Perovskite(thin film)	17.9 ± 0.8④	0.0937 (ap)	KRICT
Organic (thin film)	11.1 ± 0.3[d]	0.159 (ap)	Mitsubishi Chemical

① ap, aperture area; da, designated illumination area.

② Stability not invested. References (Asghar *et al.* and Opara Krašovec *et al.*) review the stability of similar devices.

③ Stability not invested.

④ Stability not invested.

military, and POP smart labels, posters indoors depending on opportunities, technical developments and competition.[17]

Despite many attractive features of this emerging technology, the transition from laboratory to marketplace has been hampered by a number of issues.[18] Factors affecting long-term stability are dye desorption,[19] decrease in the tri-iodide concentration,[20] degradation at the photo-electrode[21] and counter electrode[22], effect of ultraviolet light and moisture[23] and issues related to sealing.[24] Notably, poor device stability from using volatile liquid electrolyte necessitating expensive cell-sealing techniques and poor stability of sensitizing dye are crucial factors remained unresolved for DSSCs.[25]

The liquid electrolyte usually employed in DSSCs has good ionic mobility and provides high photo-to-current conversion efficiency, but it is one of the intrinsic limitations for long-term stability and reliable encapsulation because of the potential for evaporation or leakage.[26] This property also restricts its application in diverse flexible and wearable devices. Overcoming the limitations of liquid electrolytes has been the focus of considerable efforts,[27] many of which have aimed at replacing the liquid electrolyte with a polymer electrolyte,[28] inorganic p-type semiconductor,[29] or organic hole transport material.[30]

Recent research has reported that a higher photo-to-current conversion efficiency has been attained at DSSCs sensitized with porphyrin dye than at DSSCs with ruthenium dye. The redox couple incorporated into the electrolyte of DSSCs with the porphyrin dye has also changed from I^-/I_3^- to $cobalt^{(II/III)}$ in accordance with the change in the sensitized dye; however, the electrolyte that has achieved the historic high level photo-to-current conversion efficiency was still liquid type electrolyte.[31]

The decrease of J_{SC} is mainly caused by the decrease of light harvesting efficiency (η_{LH}) of sensitizing dye, which may react with I_3^- in the electrolyte,[32] be desorbed or photodegraded under illumination.[33] Ruthenium complex dye (N719) has been widely used due to high photo-conversion efficiency and proved stability.[34] However, there has been trade-off between photo-to-current conversion efficiency and long-term stability in electrolyte and UV cut-off filter.[35]

Estimating the manufacturing cost of DSSCs under the assumption of 5 % photo-to-current conversion efficiency and 5-year lifetime, leads to a levelized cost of electricity (LEC) of ¢ 49 ~ ¢ 85 /kWh. In order to achieve a more competitive COE of ¢ 7 /kWh, we would need to increase photo-to-current conversion efficiency to 15 %

and lifetime to 15 ~ 20 years.[36] The impact of lifetime on LEC is most important when the lifetime is short, while manufacturing cost is much more important when photo-to-current conversion efficiency is low.

Our objectives are increasing lifetime of DSSCs while maintaining the high photo-to-current conversion efficiency. (**Fig.6**) This effort will be needed more and more according to the achievement of higher photo-conversion efficiency in the future.[37]

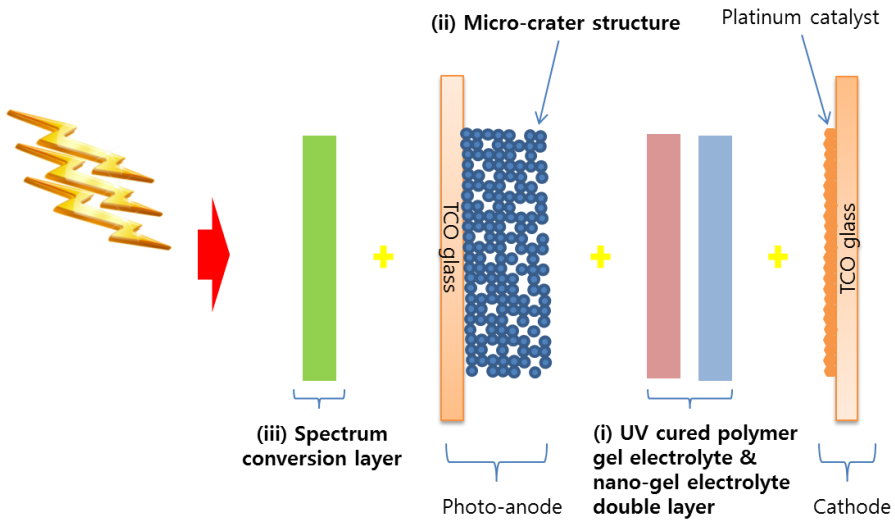

Fig. 6. Three objectives to increase the lifetime of DSSCs while maintaining the high photo-to-current conversion efficiency.

Chapter 2. Electrolyte

2.1 Current methods

Properties of electrolytes are important to increase the open circuit voltage and short circuit current. Required properties of electrolytes are as follows : close to the D^+/D energy level, sufficient driving force to regenerate the dye, good solubility, high ionic mobility, slow recombination from the photoanode and fast transfer kinetics at a minimal over potential at the counter electrode. Evaluation methods of electrolytes are nanosecond-millisecond time resolved laser photolysis studies, electro-chemical impedance spectroscopy (EIS), intensity modulated photovoltage spectroscopy (IMVS) and intensity modulated photocurrent spectroscopy (IMPS).

DSSCs using liquid electrolyte demonstrate high photo-to-current conversion efficiency, while have challenges of leakage and vaporization of organic solvent. Therefore, solidification of electrolyte using ionic liquid and gel type polymer electrolyte is crucial research direction to deal with the challenge of liquid electrolyte.

Possible alternatives for liquid electrolyte are solid organic hole conductors, inorganic p-type salts, room temperature ionic liquids, and

polymer/gel electrolytes. Solid state hole conductors are more robust, but photo-to-current conversion efficiencies are lower due to difficulties in filling tortuous pore network and faster recombination. Room temperature ionic liquids does not use solvent but show lower ionic mobility. Useful polymer/gel type electrolytes are UV cured-polymer gel electrolyte and Nano-gel electrolyte.

The use of UV-cured polymer gel electrolytes appear to have resulted in some success in terms of photo-to-current conversion efficiency due to the improved penetration of the electrolyte solution into the porous TiO_2 electrode and better interfacial contacts with the TiO_2 electrodes. This process can improve the stability of DSSCs by screen printing the electrolyte without injecting liquid electrolytes followed by short time UV curing.

In general, most of the gel type electrolytes cannot overcome the limitations of solvent leakage or evaporation because these electrolytes contain a large quantity of solvent. However, UV-cured polymer gel electrolytes have cross-linked polymers that help to trap the liquid electrolyte within the polymer matrix under sunlight irradiation and that retain their original conformation at a relatively high temperature. Despite physical advantages of gel type electrolytes, increasing the photo-to-current conversion efficiency of gel type

electrolytes including UV-cured polymer gel electrolytes to levels comparable to those of high performance liquid electrolyte remains still difficult because of the lower ionic mobility that inherently arises from the higher viscosity of the gel.[38]

Attempts to enhance the photo-to-current conversion efficiency of the DSSCs with UV-cured polymer gel electrolytes are reflected in various efforts aimed at increasing the ionic conductivity. Although these DSSCs have shown increased short circuit current values and fill factors, the increased ionic conductivity also caused back electron transfers from the TiO_2 conduction band to the I_3^- ions in the electrolyte and decreased open circuit voltage. This effect has been a limit to the performance enhancement of the UV-cured polymer gel electrolyte at a level comparable to a high performance liquid electrolyte.

2.2 New fabrication method

We address this issue by introducing a novel DSSC that incorporates a double layer gel type electrolyte. In our DSSC, a UV-cured polymer gel electrolyte layer reduces the back electron transfer from the TiO_2 conduction band to the I_3^- ions in the electrolyte, while an additional nano-gel electrolyte layer enhances the short circuit current values due to the high ionic conductivity and low charge transfer resistance between the nano-gel electrolyte and the Pt catalyst interface. We first introduce a UV-cured polymer gel electrolyte layer formed by UV-curing of the composites; this consists of the liquid electrolyte and aliphatic urethane acrylate.

Possible nanopowders that can be used in ionic liquid based electrolyte are silica, alumina, and magnesia. Zeta potentials of silica-MPN, alumina-MPN and magnesia-MPN are -48.24 mV, -15.13 mV and 34.68 mV, respectively. Charge transfer resistance is minimum in silica nanopowder loaded ionic liquid electrolyte due to attracting cation by the most negative zeta potential and facilitating high density iodide/triiodide ionic transport channels outside the nanopowders.

Liquid electrolytes were prepared by dissolving 0.05M I_2, 0.1M LiI, 0.48M TBP, 0.12M NaSCN, and 0.6M BMII in

methoxypropionitrile. UV-cured polymer gel electrolytes were prepared by the addition of UV-curable polyurethane acrylate in the prepared liquid electrolyte at 12:10 weight ratio followed by addition of 5 wt% photo initiator in the total solution. The system was continuously stirred at 60 ℃ for 12h in order to obtain a homogeneous solution.

Several types of weight ratios were tested, but when the weight ratio was less than 10:12, difficulties arose in filming on the dye-sensitized TiO_2 electrode, and when the weight ratio was more than 10:12, a noticeable decrease occurred in the photo-to-current conversion efficiency of the dye-sensitized solar cell.

Aliphatic urethane acrylate (Sartomer co.) is an aliphatic urethane with acrylates at the ends; these are cross-linked by accepting radicals from a photo initiator (1-Hydroxy-cyclohexyl-phenyl-ketone, Mw=204.3g/mole, BASF) under UV irradiation (1kW for 30 s) (see the **Fig. 7**). The use of this UV-cured polymer gel electrolyte layer enhanced the open-circuit voltage (V_{OC}) and long-term stability, especially at high temperature under light illumination.

The increase in V_{OC} can be explained in terms of the decrease in the back electron transfer from the TiO_2 conduction band to the I_3^- ions in the electrolyte, according to **Eq.(1)**.[39]

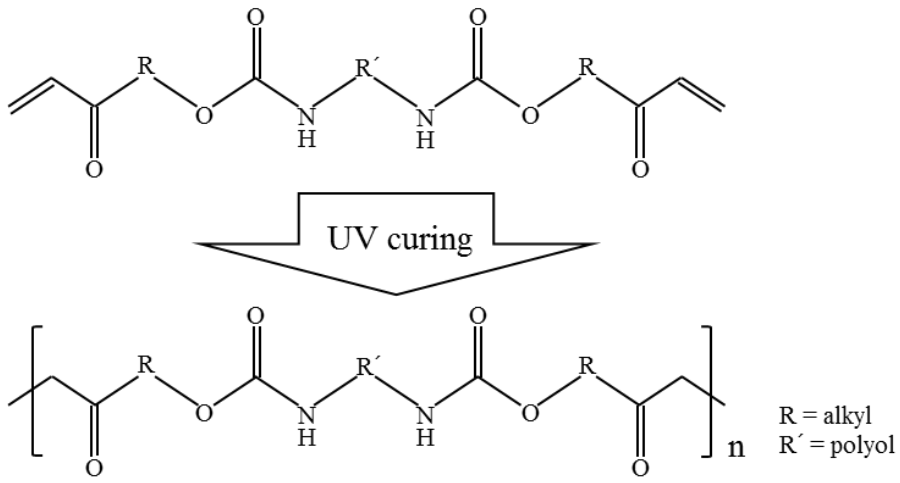

Fig. 7. UV-cured polyurethane matrix.

$$V_{oc} = \frac{kT}{e}\ln\left(I_{inj} / (n_{cb} k_{ct} [I_3^-])\right) \quad \cdots\cdots\cdots\cdots\cdots\cdots \quad (1)$$

where, I_{inj} is the charge flux from dye sensitized injection, n_{cb} is the surface electron concentration at the TiO_2 surface, and k_{ct} is the rate constant of the I_3^- reduction reaction. Use of the UV-cured polymer gel electrolyte layer at photo-anode side lowers the I_3^- ion concentration at the TiO_2 surface due to the presence of polyurethane between them and slow diffusion rate from the other place in the gel electrolyte medium.

On the other hand, a lower concentration of the I_3^- ion at the interface of the electrolyte/Pt catalyst on the counter electrode causes a higher charge transfer resistance and a slower diffusion rate in the UV-cured gel electrolyte medium lowers the short circuit current value of the DSSCs. Resolution of these problems, while maintaining the advantage of UV-cured polymer electrolyte layer, requires an additional gel type electrolyte layer with high ionic conductivity between the UV-cured polymer gel electrolyte layer and the counter electrode.

To address this issue, we suggested the gel type double layer electrolyte incorporated a nano-gel electrolyte layer, which is gelated by the simple addition of nanoparticles to an ionic liquid based

electrolyte. The role of this additional nano-gel electrolyte layer is to achieve a high photo-to-current conversion efficiency by decreasing the charge transfer resistance at the interface of the electrolyte/Pt catalyst on the counter electrode. The nano-gel electrolyte itself is a composite electrolyte consisting of an ionic liquid based electrolyte and nanoparticles. We used 1-Butyl-3-methylimidazolium iodide (BMII) as the ionic liquid and fumed silica nanoparticles (12 nm size) at a ratio of 7 wt.%. We tested several weight ratios: the viscosity was too low below 7 wt.%, and it was difficult to mix completely over 7 wt.%.[40]

A micro phase separation occurs to form the continuous paths of I^-/I_3^- rich regions; this is a result of the structure of the nanoparticles surrounded by the oppositely charged ions and I^-/I_3^- redox couples outside in the electrolyte.[41] In case of the silica nanoparticles, the zeta potential is sufficiently negative to pull the cation to the center and surround it by the I^-/I_3^- redox couple at the outside. The I^-/I_3^- rich region in the nano-gel electrolyte decreases the charge transfer resistance at the interface of the electrolyte/Pt catalyst on the counter electrode by inducing direct contact of the I^-/I_3^- redox couple with the Pt catalyst for the electrochemical reaction.[42]

When physical diffusion and exchange-reaction-based diffusion

are conjugated by an uneven concentration gradient, the total apparent diffusion coefficient can be expressed by the sum of the physical diffusion coefficient and the exchange-reaction-based diffusion coefficient, as shown in the **Eq.(2)**.[43]

$$D_{app} = D_{phys} + D_{ex} \quad \text{and} \quad D_{ex} = 1/6\, k_{ex}\, \delta^2 \mathrm{c} \qquad \text{.....(2)}$$

where, D_{app} is the apparent diffusion coefficient, D_{phys} is the physical diffusion coefficient, D_{ex} is the exchange-reaction-based diffusion coefficient, k_{ex} is the exchange-reaction rate constant, δ is the center-to-center intersite distance at the exchange reaction, and c is the concentration of the redox couple. When a silica nanoparticle forms a high I^-/I_3^- concentration region and a continuous channel surrounds the nanoparticles, the exchange-reaction-based diffusion coefficient, D_{ex}, increases proportionally to the concentration of the redox couple and enhances the apparent diffusion coefficient, D_{app}, as a result.

From our point of view, we wanted to fabricate a novel electrolyte that would have both these two advantages; therefore, we made a double layer gel type electrolyte where each layer has its own role. To demonstrate the high performance of this novel double layer gel type electrolyte, we prepared the dye-sensitized solar cells with four different electrolytes: one is solely liquid electrolyte and the others are different gel type electrolytes; nano-gel electrolyte only,

UV-cured polymer gel electrolyte only, and nano-gel electrolyte on the UV-cured polymer gel electrolyte. (**Fig. 8**, **Fig. 9**)

The fabrication process for the DSSCs with the double layer gel type electrolyte is shown in **Fig. 10**. A porous TiO_2 film with an area of 0.20 cm^2 (5mm × 4mm) was deposited on the transparent conductive glass plate by the screen-printing method followed by sintering at 550 ℃ for 30min in a muffle furnace. The resulting TiO_2 electrode was sensitized with Ruthenium dye by dipping in a 3×10^{-4} M ethanol solution of N719 (Solaronix) at 40 ℃ for 21h. Then, the dye sensitized TiO_2 electrode was rinsed with ethanol, dried, and was used for the fabrication of DSSCs with different type electrolytes : one liquid electrolyte and three gel electrolytes (Nano-gel, UV Polymer, Nano-gel on UV Polymer) were used.

For the fabrication of DSSCs with UV-cured Polymer gel electrolyte, the polymer gel precursor was screen printed on the dye sensitized TiO_2 film, which was then cured by subjecting it to 1kW of UV irradiation for 30 s. And, for the fabrication of the DSSCs with nano-gel electrolyte, the nano-gel was dropped on the dye sensitized TiO_2 film.

Transparent counter electrodes were prepared by screen printing Pt paste on the transparent conductive glass, followed by sintering at

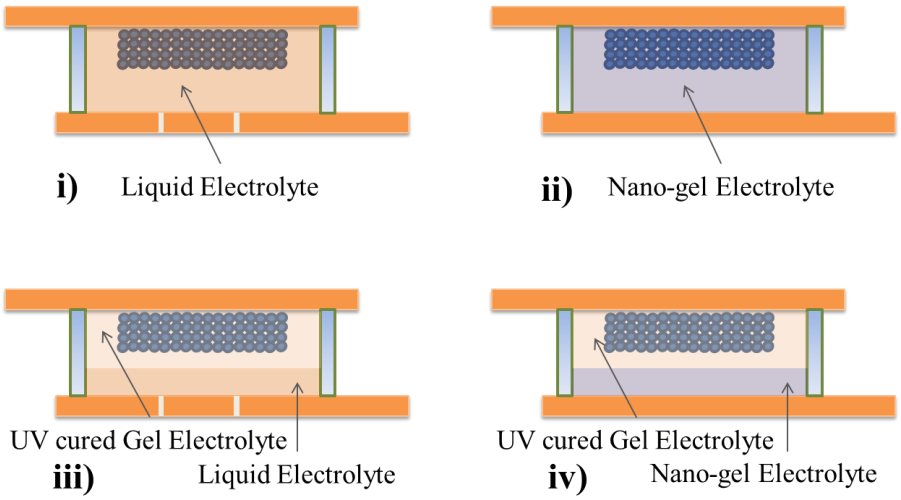

Fig. 8. Experimental scheme of DSSCs with different electrolytes.

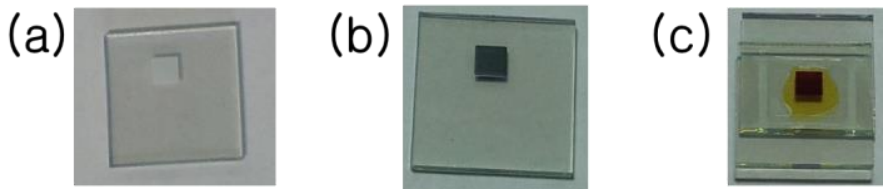

Fig. 9. (a) TiO_2 electrode, (b) TiO_2 electrode coated with UV-cured polymer gel electrolyte and (c) Assembled DSSC with nano-gel electrolyte on UV-cured polymer gel electrolyte.

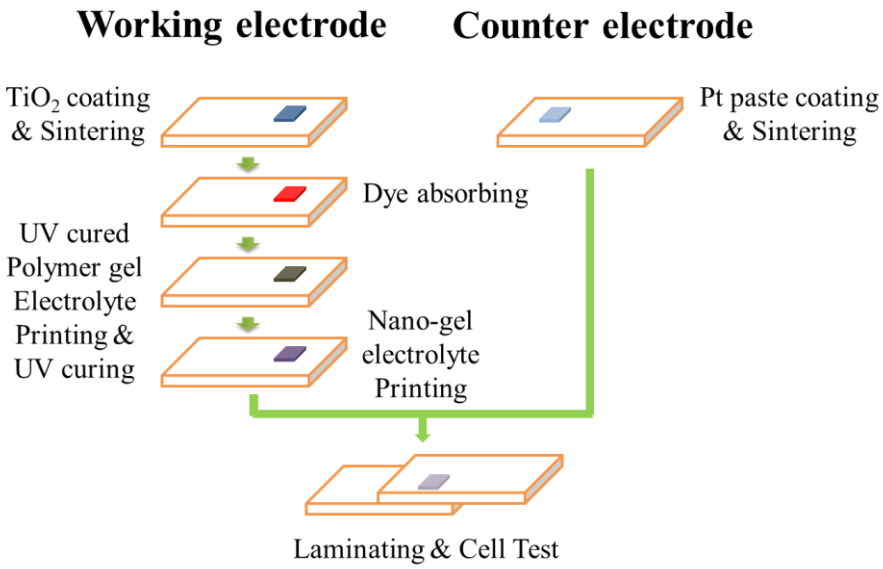

Fig. 10. DSSC Fabrication Stem using a double layer gel type electrolyte.

400 ℃ for 30min. The counter electrode was assembled with the working electrode and they were separated by 60 μm Surlyn film and then sealed by heating.

(A) Materials

All of the chemicals in this study were purchased and used without further purification. UV-curable polyurethane acrylate (Aliphatic Urethane Acrylate) was purchased from Sartomer co. and Photo initiator 1-Hydroxy-cyclohexyl-phenyl-ketone (Mw=204.3g/mole, Irgacure 184) was purchased from BASF. Iodine (I_2, 99.8%), Lithium iodide (LiI, 99%), 4-*tert*-Butylpyridine (TBP, 96%), Sodium thiocyanate (NaSCN, 98%) and 3-Methoxypropionitrile (MPN, 98%) were purchased from Aldrich. 1-Butyl-3-methylimidazolium iodide (BMII) was purchased from C-TRI. Fumed silica nanoparticles (Aerosil200) were purchased from Evonik Industries AG.

The transparent conductive glass plates (Pilkington TEC 8, Thickness 2.3 mm) were purchased from Nippon Sheet Glass co. and sensitizing dye $RuL_2(NCS)_2$:2TBA (where L=2,2´-bipyridyl-4,4´-dicarboxylic acid; TBA=tetrabutylammonium) was purchased from Ohyoung Industrial Co. TiO_2 paste (Ti-Nanoxide T), Pt paste (Platisol T/SP) and Surlyn film (Meltonix 1170-60) were purchased from Solaronix.

(B) Preparation of electrolytes

Liquid electrolytes were prepared by dissolving 0.05M I_2, 0.1M LiI, 0.48M TBP, 0.12M NaSCN, and 0.6M BMII in Methoxypropionitrile. The system was continuously stirred at room temperature for 12h in order to obtain a homogeneous solution.

Polymer gel electrolytes were prepared by the addition of UV-curable polyurethane acrylate in Liquid electrolyte at 12:10 weight ratio and the addition of 5 wt% Photo initiator in the total solution. The system was continuously stirred at 60 ℃ for 12h in order to obtain a homogeneous solution.

Nano-gel electrolytes were prepared by the addition of 7 wt% fumed silica nanoparticles in the Liquid electrolyte described above. The system was continuously stirred at room temperature for 1h in order to obtain a homogeneous one.

(C) Fabrication of DSSCs

A porous TiO_2 film with an area of 0.20 cm^2 (5mm × 4mm) was deposited on the transparent conductive glass plate by the screen-printing method followed by sintering at 550℃ for 30min in a muffle furnace. The resulting TiO_2 electrode was sensitized with Ruthenium dye by dipping in a 3×10^{-4} M ethanol solution of N719 (Solaronix) at 40 ℃ for 21h. Then, the dye sensitized TiO_2 electrode was rinsed with ethanol, dried, and was used for the fabrication of DSSCs with different type electrolytes.

Four electrolytes, one liquid electrolyte and three gel electrolytes (Nano-gel, UV Polymer, Nano-gel on UV Polymer) were used.

For the fabrication of DSSCs with UV-cured Polymer gel electrolyte, the polymer gel precursor was screen printed on the dye sensitized TiO_2 film, which was then cured by subjecting it to 1kW of UV irradiation for 30 s. And, for the fabrication of the DSSCs with nano-gel electrolyte, the nano-gel was dropped on the dye sensitized TiO_2 film.

Transparent counter electrodes were prepared by screen printing Pt paste on the transparent conductive glass, followed by sintering at 400 ℃ for 30min. The counter electrode was assembled with the

working electrode and they were separated by 60 μm Surlyn film and then sealed by heating.

(D) Measurements

Photovoltaic performance of DSSCs was evaluated using a 1600W Ozone free lamp with a ‘Class A’ Air Mass 1.5G filter in a solar simulator (Newport-94083A) and an exposure control instrument (Newport-68951) at conditions of input power 100mW/cm^2, delay time 100ms in reverse scan direction and temperature 25℃.

Incident photon-to-current conversion efficiency (IPCE%) values have been measured by illumination of the samples with a 200W Xenon Arc light sources through a filter monochromator and optical chopper in the absence of bias light (Newport-CS260). The lamp spectrum over the 350~1100 nm range satisfactorily simulates solar radiation at the surface of the earth. A dual channel Merlin lock-in amplifier was utilized for the sensitive optical power and current measurements, which comes with a built-in chopper controller in order to control optical chopper with one two-aperture blade. (Newport-QE-PV-SI)

Electrochemical Impedance measurements of the DSSCs were recorded with an EIS potentiostat (McScience-K3400) under the conditions of blue LED 460 nm, photon flux 2.36 × 10^{17}/ cm^2·S, intensity 0.1 mW/cm^2, applied bias 0.5 V, applied ac amplitude 10mV,

and the frequency range from 1000Hz to 0.5Hz.

Intensity-modulated photovoltage spectroscopy (IMVS) was recorded with an Optical Impedance measurement system (McScience-K3400) under the conditions of blue LED 460 nm, photon flux $2.36\times10^{17}/cm^2\cdot S$, intensity 0.1 mW/cm^2, applied bias 0.5V, applied ac amplitude 10mV, and the frequency range from 1000Hz to 0.5Hz.

In light-soaking tests, the cells were irradiated at open circuit using a 1000W Xenon Arc lamp at conditions of 100 mW/cm^2 with an Air Mass 1.5G filter and ambient temperature (McScience-K201).

2.3 Properties and stability

The photo-to-current conversion efficiencies of the DSSCs using different electrolytes were studied using a 1600W Ozone free lamp with a 'Class A' Air Mass (AM) 1.5G filter in a solar simulator (Newport-94083A) and an exposure control instrument (Newport-68951) at conditions of input power 100mW/ cm^2, delay time 100ms in reverse scan direction and temperature 25℃.

Photovoltaic performances of the fresh DSSCs with different types of the electrolytes for the comparison are shown in **Fig. 11** and photovoltaic parameters are summarized in **Table 2**. In case of the DSSC with UV-cured polymer gel electrolyte, the photo-to-current conversion efficiency was conspicuously low when compared to the other DSSCs, besides the shape of the current density-voltage (*J-V*) curve was very abnormal. Nevertheless, in the case of the fresh DSSC with the additional nano-gel electrolyte layer on the UV cured polymer gel electrolyte layer, the photo-to-current conversion efficiency has increased comparable to the efficiency of DSSC with the high performance liquid electrolyte and the current density of the *J-V* curve has become more saturated at the short circuit value at the same scanning rate of the voltage.

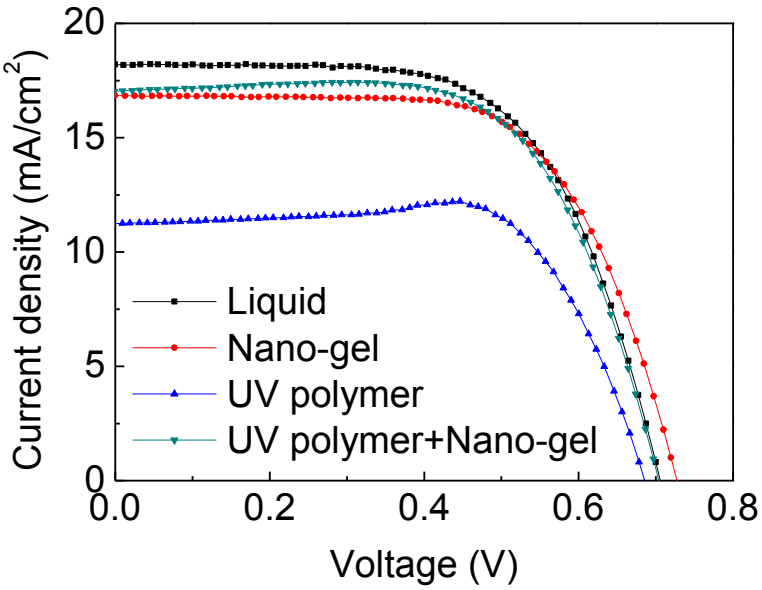

Fig. 11. Current density-Voltage (*J-V*) curves of the fresh DSSCs demonstrating initial photo-to-current conversion efficiencies according to the four different types of the electrolytes.

Table 2. Photovoltaic parameters of the fresh DSSCs with different electrolytes for the comparison and measured at room temperature under 100 mW/cm^2 AM 1.5 conditions.

Electrolyte	V_{OC} **(V)**	J_{SC} **(mA/cm^2)**	***F/F*** **(%)**	η **(%)**
Liquid	0.720	17.4	64	8.03
Nano-gel	0.741	16.4	66	7.95
UV polymer	0.691	12.3	73	6.14
UV polymer + Nano-gel	0.715	16.7	66	7.89

The DSSC with the nano-gel electrolyte exhibited a high photo-to-current conversion efficiency, which is comparable to the efficiency of the DSSC with a high performance liquid electrolyte. This result can be explained by the high ionic conductivity of the nano-gel electrolyte due to its exchange-reaction-based diffusion in spite of the high viscosity. However, the nano-gel electrolyte itself is not stable over the long term because the silica nanoparticles become separated from the solvent and aggregated readily with each other. In this study, this shortage was compensated with UV-cured polymer gel electrolyte layer, which blocked effectively the leakage of liquid electrolyte.

Theoretically, the current value must be maximal at the short circuit state; however, in case of the fresh DSSC with the UV-cured polymer gel electrolyte, the current value is not saturated at the short circuit state, even at the slowest scanning rate of the voltage. This observation was termed “over-shoot” effect and analyzed by the previous report that the inability to sustain the photocurrent in the “fresh” device under full sun conditions is due to the charge build up at the dye/TiO_2 interface.[44] Therefore, we measured the current density-voltage curves of the fully aged DSSCs again which is shown in **Fig. 12** to demonstrate the characteristics of the fully aged DSSCs with each type of the electrolytes. Ageing times at dark state needed

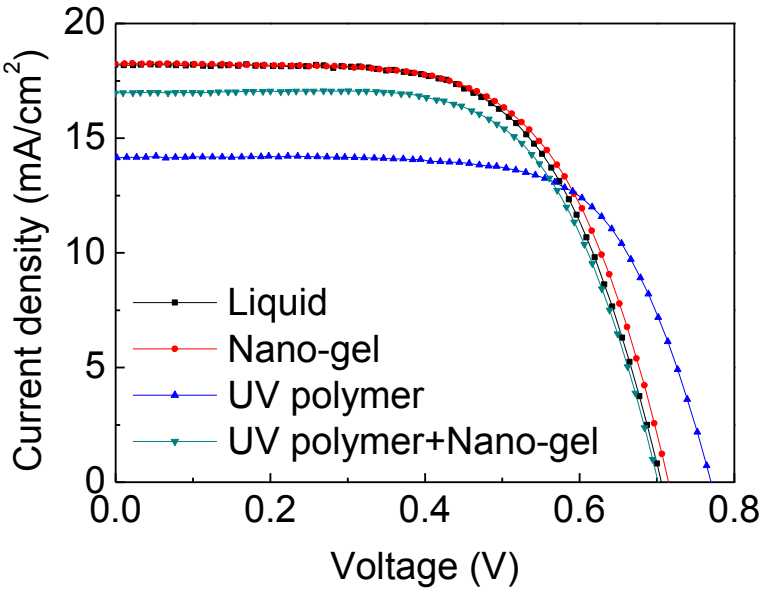

Fig. 12. Current density-Voltage (*J-V*) curves of the fully aged DSSCs demonstrating maximum photo-to-current conversion efficiencies according to the four different types of the electrolytes.

for high photo-to-current efficiencies were one day for liquid electrolyte, a few hours for Nano-gel electrolyte, three days for UV-cured polymer electrolyte, and one day for double layer gel type electrolyte with UV-cured polymer electrolyte and Nano-gel electrolyte.

Improvement of short-circuit current in DSSC using double layer electrolyte can be explained again by the effect of redox couple concentration in the ionic liquid electrolyte. In case of DSSC using liquid electrolyte incorporating redox couple, short-circuit current of DSSC can be increased through multiple electrolyte layers within limit, while DSSC using hole transport materials show decreased short-circuit current by multiple hole transport material layers.

The incident photon-to-current conversion efficiencies (IPCE) of DSSCs are used for spectral response of solar cell, which is mainly dependent on the absorption spectra of the dye sensitizers. Especially in case of small cell, it is difficult to determine an active area, but there is no need to correct active area to measure IPCE of the solar cell.

IPCE of solar cell is a sum of the short-circuit current densities (J_{ph}) generated against a sing photon with wavelength λ absorbance of the solar irradiance (Φ), as shown in the **Eq.(3)**.

$$\text{IPCE}\,(\%) = \frac{1.240 \times 10^5 \times J_{ph}}{\lambda \times \Phi} \quad \ldots\ldots\ldots\ldots\ldots\ldots \quad (3)$$

There are three factors of IPCE : (i) light harvesting efficiency related to the ability of the dye (η_{LH}), (ii) charge transfer efficiency from dye to the conduction band of TiO_2 (η_{INJ}), and (iii) charge collection efficiency to the anode avoiding recombination (η_{COL}). However, there are limitations in case of quasi-solid state DSSC due to the non-linear relationship between light intensity and photocurrent density in DC mode. Therefore, AC mode is applied to measure IPCE of quasi-solid state DSSC, but IPCE is affected by the frequency and bias light. As a result, it is not expected that the IPCE value of quasi solid state DSSC represent absolute efficiency value, although relative comparison of power generation according to the wavelength is demonstrated.

The incident photon-to-current conversion efficiencies (IPCE) of the fully aged DSSCs with different electrolyte types at a chopper frequency of 5Hz in the absence of the bias light was measured for relative comparison and exhibited relatively small differences (**Fig. 13**). The external quantum efficiencies (EQE) showed the peak wavelength value ranging between 513nm and 527nm, as shown in the **Table 3**. The EQEs at the peak wavelength value of the DSSCs

with the liquid electrolyte and the double layer gel type electrolyte showed slightly higher values compared to the values obtained with the DSSC incorporating the UV cured polymer gel electrolyte only. This result arises from lower recombination and light scattering effect. In case of double layer electrolyte, UV-cured polymer electrolyte gives low recombination effect and Nano-gel electrolyte gives light scattering effect.

The shapes of the IPCE curves are more important and show that the absorption spectrums of the DSSCs with the liquid electrolyte and the double layer gel electrolyte are analogous to one another. On the other hand, the IPCE curves of the DSSCs only with the nano-gel electrolyte or the UV-cured polymer gel electrolyte are shifted to the left slightly compared to the IPCE curve of the DSSC with the liquid electrolyte. Although, the photocurrent density values calculated from the IPCE spectra are far less than the measured values at *J-V* curves due to the high chopper frequency range and the absence of the bias light, these external quantum efficiency results are consistent with the solar energy conversion efficiency results.

In case of fully aged DSSCs with different types of electrolytes, there is little difference in efficiency value of IPCE, however, it can be improved strikingly by applying light scattering layer on the TiO_2

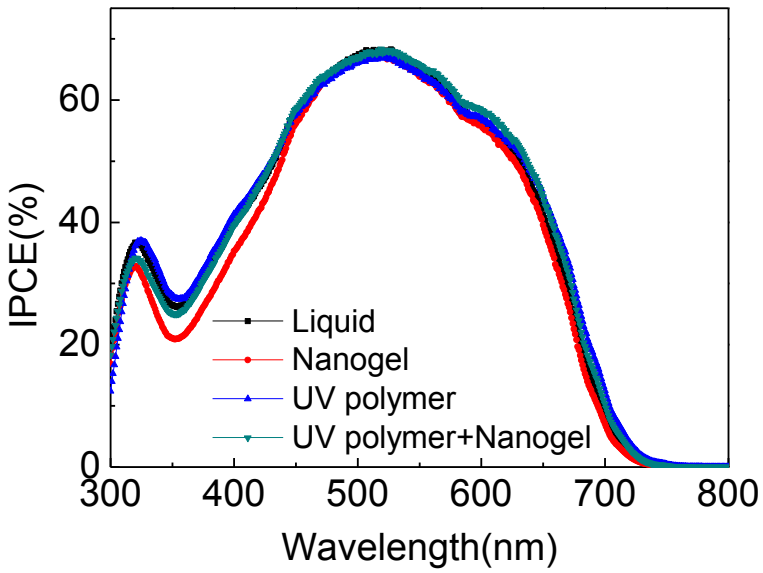

Fig. 13. The incident photon-to-current conversion efficiencies (IPCE) of the fully aged DSSCs with four different electrolytes.

Table 3. External quantum efficiencies of the fully aged DSSCs with four different electrolytes by the IPCE measurement at chopper frequency 5Hz in the absence of bias light.

	Liquid	**Nano-gel**	**UV polymer**	**UV polymer + nano-gel**
Wavelength at Peak (nm)	527	513	517	527
IPCE (%)	68.3	67.5	67.1	68.2

photoanode layer.

Electrochemical impedance measurements of the DSSCs incorporating different electrolytes are shown in **Fig. 14**. EIS measurements were recorded with an EIS potentiostat (McScience-K3400) under the conditions of blue LED 460 nm, photon flux 2.36 × 10^{17}/ cm^2·S, intensity 0.1 mW/cm^2, applied bias 0.5 V, applied ac amplitude 10 mV, and the frequency range from 1000 Hz to 0.5 Hz.

Research on the charge-transfer reaction at the platinum electrode in a dark condition from a symmetrical cell indicates that the impedance values at a frequency range between 100 Hz and 10 kHz are related to the charge transfer resistance at the Pt counter electrode.[45] Among the four different types of electrolytes tested in this study, the liquid electrolyte had the smallest impedance value, followed by the nano-gel electrolyte (which has a high ionic conductivity due to the micro-phase separation effect of the silica nanoparticles). In contrast, the UV-cured polymer gel electrolyte had the largest impedance, mainly due to the larger charge transfer resistance between the electrolyte and the platinum electrode interface. The double layer gel type electrolyte had a lower charge transfer resistance than the UV-cured polymer gel electrolyte itself, due to the effect of the nano-gel electrolyte layer located at the Pt counter

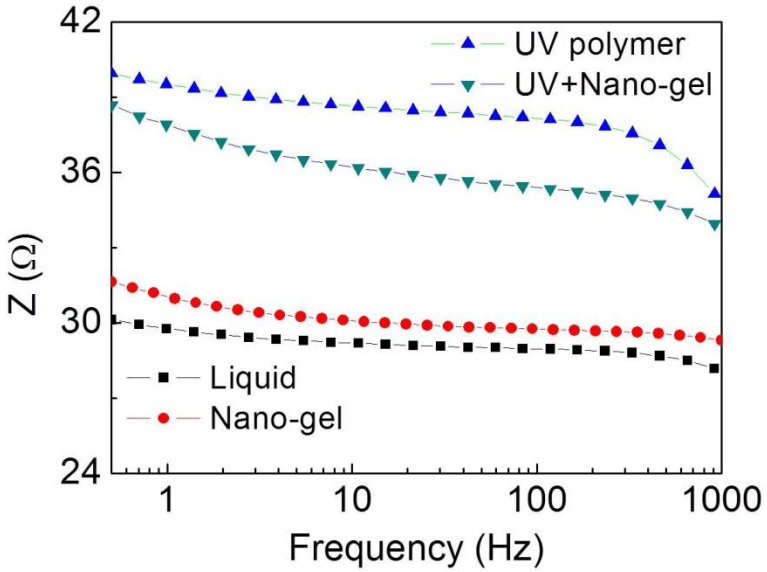

Fig. 14. Electrochemical Impedance measurement result of the DSSCs with four different electrolytes under light condition.

electrode and induced the improvement of short circuit current level. Intensity-modulated photovoltage spectroscopy (IMVS) measurement results for the DSSCs incorporating different electrolytes are shown in **Fig. 15**. The shapes of the IMVS curves were divided into two groups: one group was a DSSC with a liquid electrolyte and the other group was DSSCs with the three gel type electrolytes. As shown in the figure, all the curves of the DSSCs with the three gel type electrolytes coincided with each other and had the same IMVS values.

The liquid electrolyte had a frequency at the maximum photo voltage point of 1.098 Hz and the electron recombination lifetime was 145 ms. On the other hand, the three gel type electrolytes, regardless of their types, all showed frequencies at the maximum photo voltage point of 0.845 Hz and the electron recombination lifetimes were all 188 ms. In this study, note that the electron recombination at the TiO_2 conduction band can be reduced about 30% by substituting the liquid electrolyte with gel electrolyte irrespective of gel types.

We investigated the stability of the DSSCs with different electrolytes by light soaking tests. The solar cells were light illuminated continuously at the open circuit condition using the Xenon lamp of a solar simulator without an optical filter at an incident light intensity of 100 mW/cm^2. The photo-to-current conversion

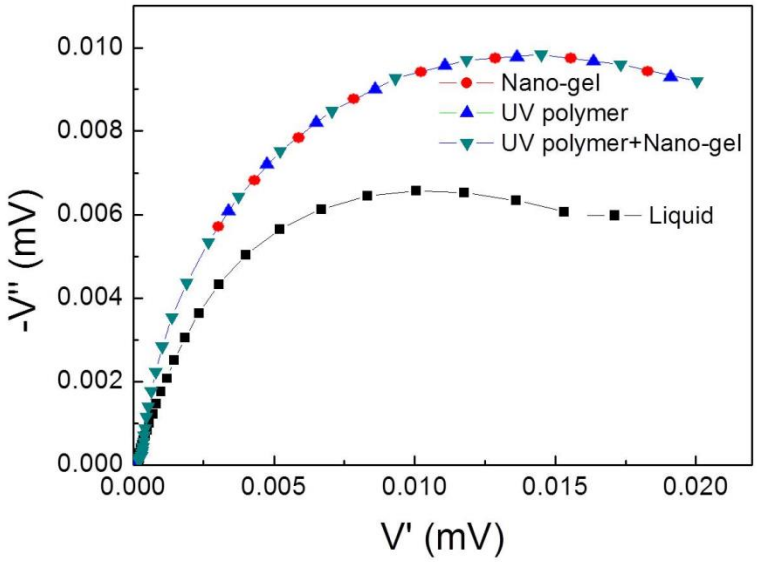

Fig. 15. IMVS measurement result of the DSSCs with four different electrolytes under light condition.

efficiencies were measured for 24 hours.

Fig. 16 shows the stabilities of the fully aged DSSC with the liquid electrolyte and the DSSCs with the gel type electrolytes under light illumination conditions without an optical filter. Photovoltaic performances at light-soaking test are shown in **Table 4**. The DSSC with the nano-gel electrolyte had the best efficiency at first due to high ionic conductivity and decreased charge transfer resistance, but the efficiency dropped quickly due to the easy separation and aggregation of the silica nanoparticles from the solvent. The efficiency of the DSSC with the liquid electrolyte increased for one day, but decreased gradually during the continuous light illumination. The efficiency of the DSSC with the UV-cured polymer gel electrolyte increased slowly for three days, reaching higher efficiency by the effect of decreased recombination and three-dimensional arrangement of polyurethane-I_2 complex, and then decreased more slowly than the DSSC with the liquid electrolyte.

The DSSC fabricated with the double layer gel type electrolyte exhibited a photo-to-current conversion efficiency of 7.89%, which is comparable to the value of 8.03% of the high performance liquid electrolyte after a one day stabilization period. Furthermore, the marked enhancement of the stability was confirmed by the retention of

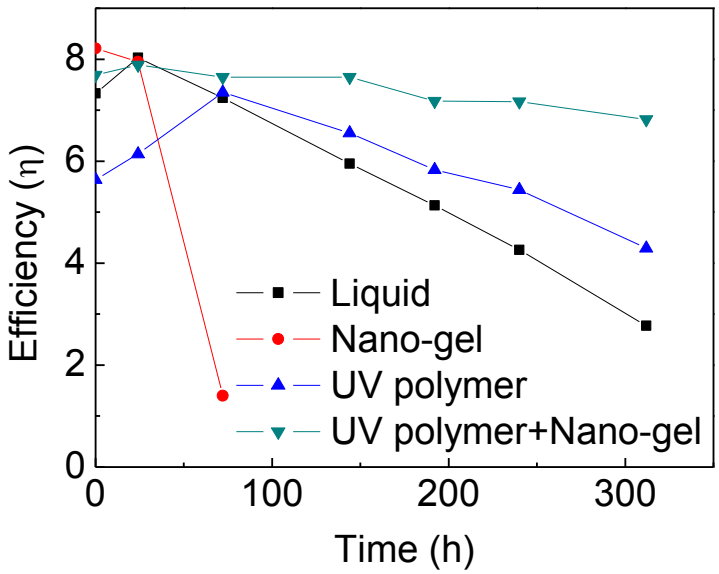

Fig. 16. Light-soaking test results of fully aged DSSCs with a liquid electrolyte and three different gel type electrolytes.

Table 4. Photovoltaic performances of the fully aged DSSCs with a liquid electrolyte and three different gel type electrolytes at light-soaking test.

Electrolyte	0 hour	72 hour	192 hour	312 hour
Liquid	7.33	7.24	5.13	2.77
Nano-gel	8.21	1.40	-	-
UV polymer	5.64	7.35	5.83	4.29
UV polymer + nano-gel	7.69	7.65	7.18	6.82

the efficiency at 6.82% compared to 2.77% for the high performance liquid electrolyte and 4.29% for the UV-cured polymer gel electrolyte after two weeks of continuous light soaking without an optical filter.

2.4 Conclusions

A novel method of fabricating DSSCs with a double layer gel type electrolyte was introduced to overcome the photo-to-current conversion efficiency limitation of the gel type electrolyte while maintaining a long-term stability. In a double layer gel type electrolyte, a UV-cured polymer gel electrolyte was used as a high stability layer on the TiO_2 nano porous film and an additional nano-gel electrolyte layer comprised of silica nanoparticles and ionic liquid was used as a photo-to-current conversion efficiency enhancing layer, which increased ionic conductivity and decreased the charge transfer resistance at the platinum counter electrode. Also, the influence of the double layer gel type electrolyte was investigated by photo-to-current conversion efficiency measurements and a continuous light soaking test without an optical filter.

Introduction of an additional nano-gel electrolyte layer onto the UV-cured polymer gel electrolyte layer in the DSSC resulted in the marked enhancement of the device efficiency and stability. The photo-to-current conversion efficiency was 7.89% after one day stabilization period and was maintained at 6.82% even after two weeks of continuous light-soaking without an optical filter. This confirms a 2.5

times higher long term performance of the double layer gel type electrolyte compared to the high performance of a solely liquid electrolyte. We believe that this double layer gel type electrolyte shows a good potential, which can meet various needs of next-generation high-performance DSSCs.

Chapter 3. TiO_2 film structure

3.1 Current methods

Conventional TiO_2 film structure consists of light scattering layer incorporating ca. 400~500 nm TiO_2 nanoparticles.on the top of the nanocrystalline TiO_2 layer incorporating ca. 20 nm nanoparticles. This light scattering layer diffuses incident light to dyes for higher light absorption and power generation. However, the fabrication process is complicated to deposit additional scattering layer, while the light scattering effect is not satisfactory compared to hierarchical mirco-porous nanocrystalline TiO_2 film.

For effective light harvesting in DSSCs, hierarchical micro-porous nanocrystalline TiO_2 films were introduced via hard- and soft-templating routes.[46] The hard-templating synthesis is commonly used to fabricate ordered three-dimensional (3D) TiO_2 porous structures with crystalline framework, high specific surface area, and tailored pore structure. This templating route involves the use of colloidal particles, polymeric beads, and anodic alumina membranes, thereafter, these templates would be removed to generate unique porous materials. The soft-templating synthesis involves the use of

organic or polymeric surfactants which self-assemble into a diversity of supermolecular structures, including spherical micelles, hexagonal rods, lamellar, and other structures in solution, which are used as soft templates to tune the structure and size of pores in TiO_2 materials.[47]

Use of the hierarchical micro-porous TiO_2 films had the merits of improved light scattering effect for enhanced performance of DSSCs. In addition, the large pin holes on the surface improved the infiltration process of gel-type electrolyte into the TiO_2 films.[48] However, achieving both purposes simultaneously with simple fabrication method to facilitate micro-crater structure for wide channel of gel-type electrolyte and nano-pores for light scattering effect are great challenges until now.

3.2 New fabrication method

In the present study, we exerted ourselves to find an optimal hierarchical TiO_2 photo-anode morphology tailored for the gel-type electrolyte DSSCs by simply adding high temperature volatile material in the TiO_2 paste without using cumbersome hard or soft template. To prepare a micro-crater structure, acetylene-black (hereafter referred to as AB) was blended into the TiO_2 paste, thereafter, evaporated at high temperature of sintering process. Sensitized dye was adhered onto the TiO_2 surface, and then gel-type electrolyte was infiltrated into the micro-crater shaped pores in the TiO_2 film. (see **Fig. 17**)

To find the optimal light scattering condition in micro-crater structures, the changes of optical properties of the TiO_2 photo-anode films according to the formation of hierarchical micro-crater morphology by the addition and evaporation of AB at high temperature were analyzed using spectrophotometer. Also, the photovoltaic performance and long-term stability of the prepared DSSCs incorporating double layer gel-type electrolyte were studied using solar simulator and IPCE measurement system. This method demonstrated 8.7 % photo-conversion efficiency without using

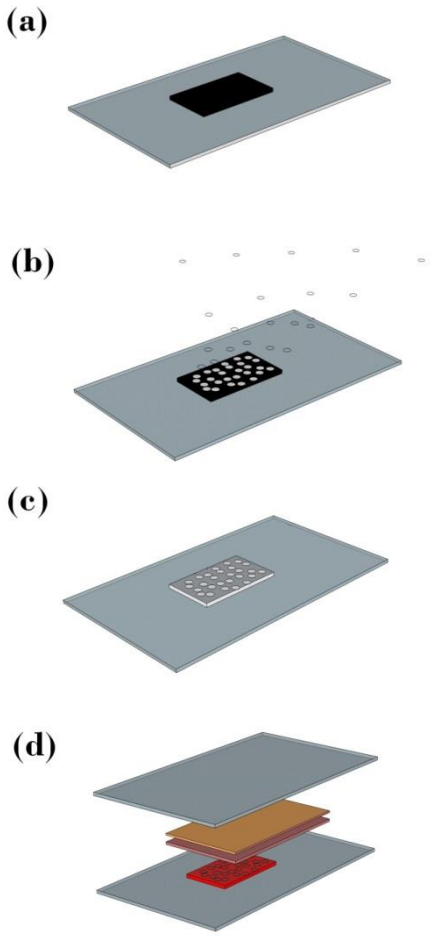

Fig. 17. Novel fabrication process using TiO_2 photo-anode film with acetylene-black for double layer gel-type electrolyte DSSC (a) TiO_2 film on FTO glass (b) evaporation of acetylene-black at high temperature treatment (c) hierarchical micro porous structure formation and (d) fabrication of double layer gel-type electrolyte between the the two electrode glasses.

additional light scattering layer, which is around 10% higher than the method fabricating TiO_2 film without adding AB in the TiO_2 paste.

TiO_2 nanoparticles were synthesized by using the hydrothermal method.[49] Tetrabutyl titanate (10 mL), butanol (60 mL), acetone (10 mL), and acetic acid (10 mL) were mixed. A mixture of butanol (40 mL) and distilled water (3 mL) was then added to the above solution, followed by stirring for 1h and the hydrothermal process at 240 ℃ for 6 hours in an autoclave. The mixture was cooled at room temperature and enriched using a rotary-evaporator in 13 % TiO_2 colloid.

TiO_2 pastes (hereafter referred to as Normal TiO_2 pastes) were prepared by the combustion process using the TiO_2 colloid for the starting material. Ethyl cellulose was added for the binder, and terpineol for the solvent of the TiO_2 colloidal solution, followed by a mixing process using a paste blender. Then, to facilitate a formation of micro-crater structure on the TiO_2 photo-anode films, TiO_2 pastes containing AB (hereafter referred to as AB TiO_2 pastes) were prepared using a paste-blending method in the reference.[50]

To compare the optical properties between the TiO_2 films with (referred to as AB TiO_2 film) and without AB (referred to as Normal TiO_2 film), both TiO_2 pastes were screen printed onto the FTO glass

(TEC 8/2.3mm, 8 Ω/sq, Pilkington) in a total area of 100 × 100 mm^2 and then sintered at temperatures of 200 ℃, 450 ℃, and 550 ℃ respectively in ambient air using a muffle furnace.[51]

The transmittance, opacity, and haze of the TiO_2 photo-anodes were measured by transmittance mode, and the diffuse reflectance, and whiteness index of the TiO_2 photo-anodes were measured by reflection mode using a UV-vis spectrophotometer (CM-5 Konica Minolta, Japan) and analyzed using a color data software (SpectraMagic NX Ver.2.1 Konica Minolta, Japan).

(A) Synthesis of electrolytes

Liquid type electrolytes were prepared by dissolving 0.05M I_2, 0.1M LiI, 0.48M TBP, 0.12M NaSCN, and 0.6M BMII in methoxypropionitrile.

UV-cured polymer gel type electrolytes were prepared by the addition of UV-curable polyurethane acrylate in the liquid type electrolyte at 12:10 weight ratio with 5 wt% photo initiator in the total solution.

Nano-gel type electrolytes were prepared by the addition of 7 wt% fumed silica nanoparticles in the liquid type electrolyte as previously described.

(B) Fabrication of the DSSCs

For the fabrication of the DSSCs, TiO_2 photo-anode films were prepared by the screen printing method with aperture area of 0.2 cm^2 and then sintered at 550 ℃ for 30 minutes. Dye adsorption was carried out by dipping the TiO_2 photo-anode films into 4×10^{-4} M t-butanol/acetonitrile (Merck, 1:1) solution of the standard ruthenium dye (N719, Solaronix) for 48 hours at 25 ℃. In case of double layer gel-type electrolyte, firstly the UV-cured polymer gel type electrolyte was coated on the TiO_2 photo-anode films and then the nano-gel type electrolyte was coated later. Counter electrodes were prepared by dropping the 10 mM hydrogen hexachloroplatinate (IV) hydrate (99.9%, Aldrich) in a 2-propanol solution onto the transparent FTO glass and sintering at 400 ℃ for 30 minutes. The two electrodes were assembled and separated using thermal adhesive polymer film (Surlyn, thickness 60 ㎛).

(C) Photovoltaic characterization of the DSSCs

The photovoltaic properties of the prepared DSSCs were measured using a lamp with air mass 1.5G filter as light source in a solar simulator and an exposure control instrument (Newport). The light intensity was adjusted with a reference Si cell (Fraunhofer Institute for Solar Energy System). Photovoltaic performance was characterized by *Voc*, *Jsc*, and *FF* (fill factor), and the overall photo-to-current conversion efficiency was characterized using the current density-voltage (*J*-*V*) curve.

Incident photon-to-current conversion efficiencies (IPCE) were measured by the illumination of the prepared DSSCs with a xenon arc light sources through a filter monochromator and optical chopper at 2 Hz under bias light (Newport).

For the stability test under continuous light illumination, the prepared DSSCs were irradiated at open circuit state using a xenon arc lamp at 1 sun condition in an ambient temperature (McScience). Then, the photo-to-current conversion efficiency was characterized periodically.

3.3 Properties and stability

To find the optimal heat treatment condition of the AB TiO_2 film prepared as above procedure, optical properties were measured by spectrophotometer. **Fig. 18** shows the transmittance and opacity of the TiO_2 photo-anode films including 1.0 wt.% AB. These TiO_2 photo-anode films were heat treated at 200 and 450 ℃ for 60 minutes, and 550 ℃ for 5 minutes. Transmittance was observed to be near zero at 200 ℃ indicating no evaporation of AB. Transmittance of 35% at 450 ℃ was attributed to the partial evaporation of AB. Maximum transmittance of 67% at 550 ℃ indicates that nearly pure white color was obtained from the almost full decomposition of AB.

In this research, opacity was measured as a parameter for scattering efficiency of visible light due to the formation of hierarchical micro-porous structures in the TiO_2 photo-anode films. The difference between the refractive index of the anatase crystalline TiO_2 films (R.I. 2.55) and the air (R.I. 1) is large enough to provide a diffuse reflectance and opacity by the light-scattering. Opacity in optics is the measure of impenetrability to electromagnetic radiation, especially visible light, also termed as a mass attenuation coefficient or a mass absorption coefficient. In more special condition, if a beam

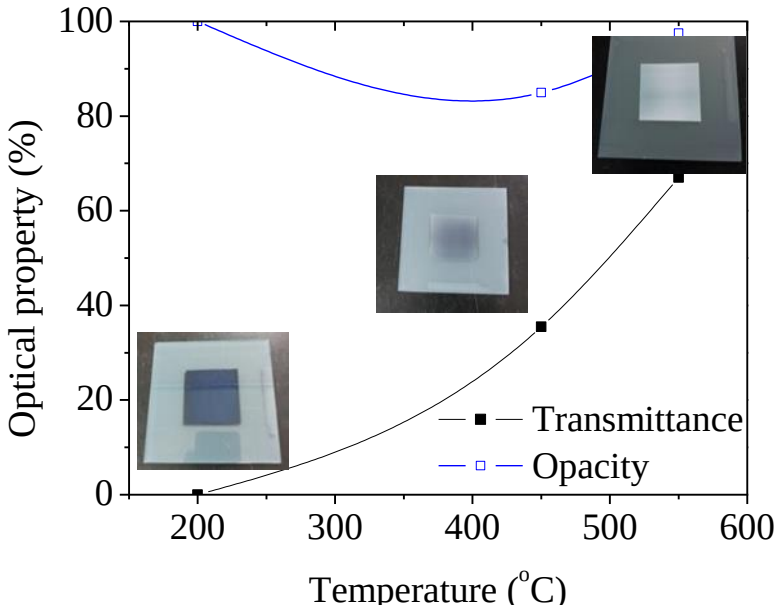

Fig. 18. Optical properties of the TiO_2 photo-anode films containing 1 wt.% of acetylene-black measured by spectrophotometer according to the heat treatment conditions of 200 ℃ for 60 minutes, 450 ℃ for 60 minutes, and 550 ℃ for 5 minutes. Each photograph images indicated inset correspond to each measured points.

of light with frequency, v, travels through a medium with constant opacity value, Kv, and constant mass density value, ρ, then the intensity will be reduced with distance, x, according to the formula

$$I(x) = I_0\ e^{-Kv\rho x} \quad \text{.....(4)}$$

where, x is the distance of the light which has travelled through the medium, $I(x)$ is the intensity of light remaining at distance x, and I_0 is the initial intensity of light, at x=0.

Opacities of the AB TiO_2 photo-anodes were measured after different heat treatment conditions. The opacity value could not be measured after 200 ℃ heat treatment due to no visible light transmission by the remaining organic materials and AB. The opacity value of 85 % after 450 ℃ heat treatment was attributed to partial evaporation of AB resulting in partial absorption and partial scattering of visible light. The maximum opacity value of 98 % after 550 ℃ heat treatment was attributed to nearly full decomposition of AB which facilitated formation of hierarchical micro-crater structure on TiO_2 photo-anode film.

In order to find an optimized heat treatment time at selected temperature, AB TiO_2 photo-anode films were prepared using different heat treatment times of 30 and 50 minutes at the optimal heat treatment temperature of 550 ℃. (see **Fig. 19**) The maximum

transmittance value of 68 % was obtained at 30 minutes heat treatment time by the more complete evaporation of AB. This result also confirmed that the more complete evaporation of AB has facilitated more effective light scattering structure. On the other hand, excess heat treatment up to 50 minutes has been proven too long to obtain an effective structure, while exhibiting the lower transmittance of 66 % and the lower opacity value of 95 % due to the excess heat treatment and loss of light scattering effect in the TiO_2 photo-anode film. Generally, the thickness of TiO_2 film decreases according to heat treatment time improving the connectivity between the TiO_2 nanoparticles. However, this increase of density in AB TiO_2 photo-anode films induces decrease of nano- and micro-pores facilitated by the evaporation of AB.

The transmittance and the opacity values shown above supported that AB was evaporated completely under the optimized heat treatment conditions facilitating the formation of effective hierarchical micro-crater TiO_2 photo-anode films for light scattering effect. To compare the optical properties variable to the wavelengths of the visible light, transmittance and diffuse reflectance were measured between the TiO_2 photo-anode films without and with AB to

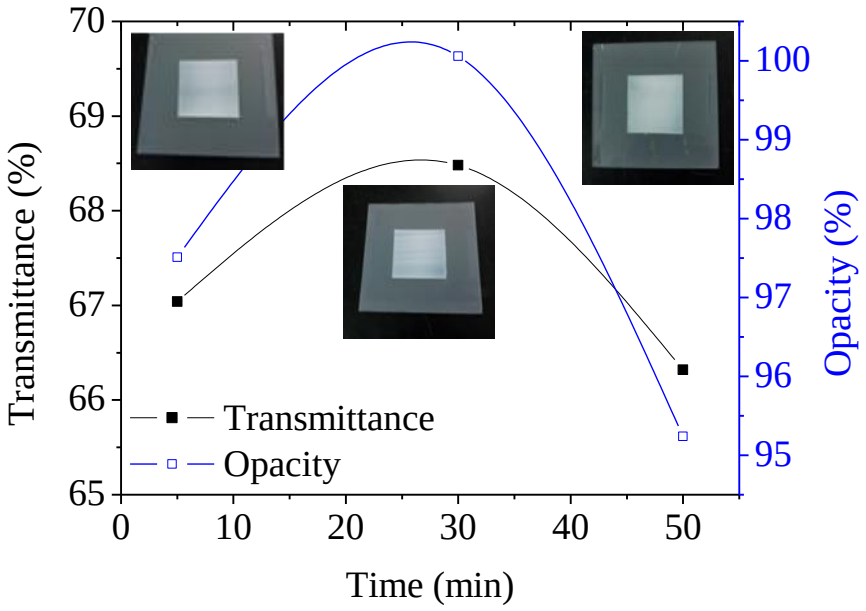

Fig. 19. Optical properties of the TiO_2 photo-anode films containing 1 wt.% of acetylene-black measured by spectrophotometer according to the heat treatment times of 5 minutes, 30 minutes, and 50 minutes at 550 ℃. Each photograph images indicated inset correspond to each measured points.

understand the wavelength range of the light scattered by the effective formation of hierarchical micro-crater structure on the TiO_2 nano-crystalline frame.

Fig. 20 shows the light transmittances in accordance with a wavelength of the bare FTO glass, Normal TiO_2 films, and AB TiO_2 films. Light transmittances at around 360 nm wavelength are near zero in case of both Normal and AB TiO_2 films due to the ultra violet light region absorbance of the TiO_2 materials, while bare FTO glasses without TiO_2 films exhibit rather higher light transmittances. Light transmittances are recovered in between 400 nm and the visible light regions relying on the thickness and light scattering effect of the Normal TiO_2 films, however, the transmittance of the AB films does not reach the analogous level of Normal films even with only one time coating thicknesses.

Fig. 21 shows the diffuse reflectance in accordance with a wavelength of the bare FTO glass, Normal TiO_2 films, and AB TiO_2 films. Diffuse reflectance at around 360 nm wavelength is near zero in case of the both Normal and AB TiO_2 films, which confirms that ultra violet light region absorptions by TiO_2 materials are dominant in that wavelength region. Peak diffuse reflectance wavelengths were found at around 400 nm in both TiO_2 films, in the meanwhile bare FTO

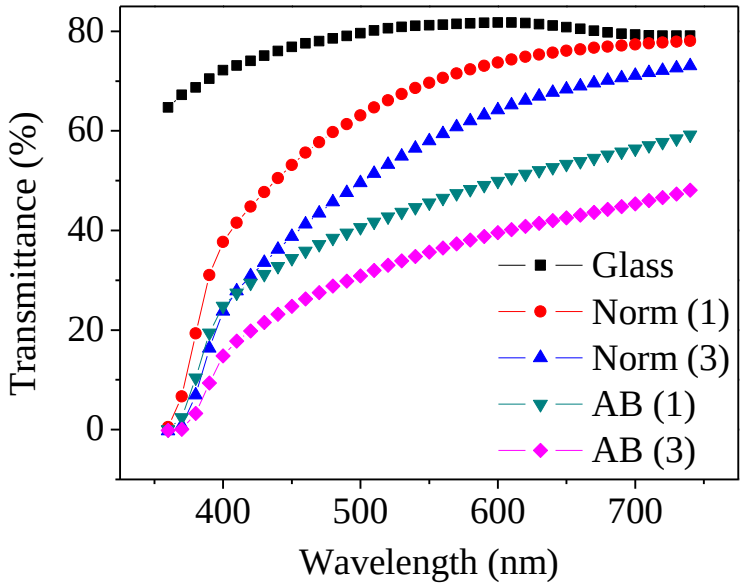

Fig. 20. Comparison of the Transmittances of the TiO_2 photo-anode films prepared as bare FTO glass, normal TiO_2 film screen printed one time or three times, AB TiO_2 film screen printed one time or three times, respectively. Here, A.B. denotes the acetylene-black.

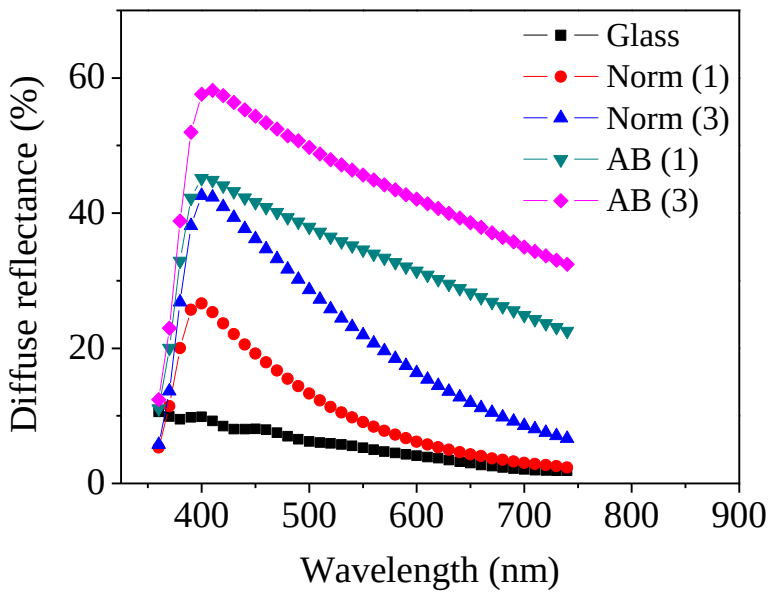

Fig. 21. Comparison of the Reflectances of the TiO_2 photo-anode films prepared as bare FTO glass, normal TiO_2 film screen printed one time or three times, AB TiO_2 film screen printed one time or three times, respectively.

glasses exhibited no diffuse reflections. Furthermore, AB films have shown rather higher diffuse reflectance in between 400 nm and visible wavelength region than Normal films, which also confirms that the recycled lights at visible wavelength region are not absorbed by the TiO_2 nano particle materials, but also diffuse reflected by the micro-crater structure.

In order to investigate the effect of the thickness of the TiO_2 films against the light scattering properties, different thickness of TiO_2 films with and without AB were prepared using screen printing method by coating 1 time or 3 times repeatedly. Scanning electron micrograph images of each photo-anode films are shown in **Fig. 22**. The thickness were 8.2 μm and 19.3 μm by 1 time and 3 time coatings in Normal TiO_2 films, and 8.3 μm and 19.6 μm by 1 time or 3 times coatings in AB TiO_2 films, respectively.

Fig. 23 shows the light transmittance, opacity, and haze values of the bare FTO glass, Normal TiO_2 film and AB TiO_2 film measured by the transmittance mode of the spectrophotometer. The light transmittances of the films decreased in proportional to the thickness or coating numbers, while exhibiting lower values in AB films compared to the Normal films.

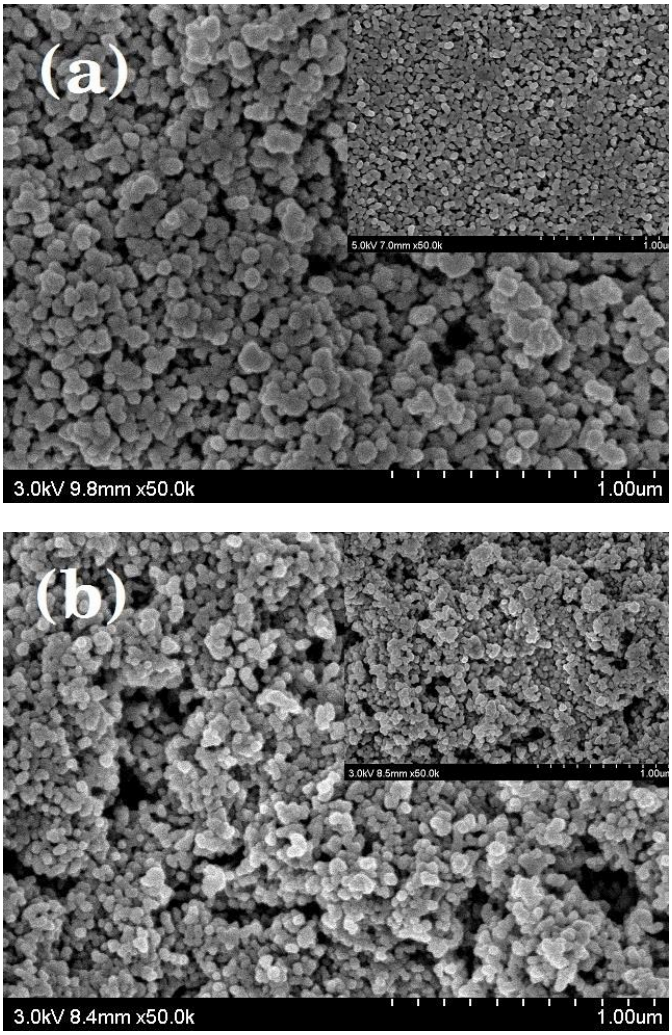

Fig. 22. Scanning electron micrograph images of (a) Normal TiO_2 photo-anode film and (b) AB TiO_2 photo-anode film. Inset images are cross-section view images, respectively.

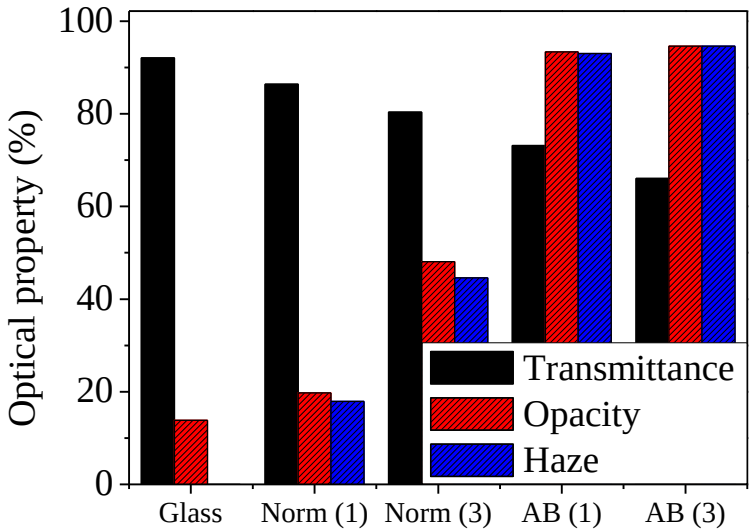

Fig. 23. Comparison of the various optical properties according to the thickness measured by Transmittance mode of the bare FTO glass, normal TiO_2 films, and AB TiO_2 films which were screen printed one time or three times, respectively.

This phenomenon can be explained directly by the increase of diffuse reflectance of the Normal and AB TiO_2 films, and the diffuse reflectance and whiteness index values measured by the reflectance mode of the spectrophotometer are shown in **Fig. 24**. From the data of the bare FTO glass, the opacity value by the transmittance mode of 14 % and the diffuse reflectance value by the reflectance mode of 27 %, we can understand that thin metal oxide layer on the transparent glass scatters or reflects the visible light fundamentally. In case of the Normal TiO_2 films, the thickness of the film was a very important parameter for the light scattering effect, exhibiting higher opacity, haze values in transmittance mode and higher diffuse reflectance, whiteness index values in reflectance mode. However, the thick films with nanoparticles have limit for an easy infiltration of the gel-type electrolyte.

In case of the AB TiO_2 films, the thickness was not a major parameter for the light scattering effect, because the formation of the hierarchical micro-crater structure was a more effective parameter. By increasing the thickness of the AB films, the opacity, haze values were not changed much and the whiteness index value increased slightly. Therefore, it is clear that the AB TiO_2 films are more effective for light recycling with thin layer than Normal TiO_2 films and the

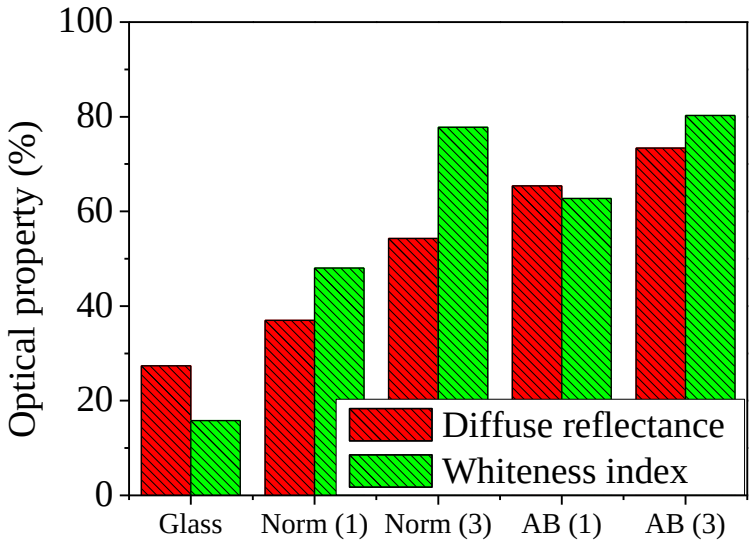

Fig. 24. Comparison of the various optical properties according to the thickness measured by Diffuse reflectance mode of the bare FTO glass, normal TiO_2 films, and AB TiO_2 films which were screen printed one time or three times, respectively.

hierarchical micro-crater structure can provide wide channels for easy infiltration of the electrolyte. The easy infiltration of the electrolyte is more important for the gel-type electrolyte having higher viscosity, which is essential to enhance the long-term stability of the DSSCs.

Photovoltaic evaluation results of the DSSCs using different types of electrolytes with AB TiO_2 photo-anode films are shown in **Fig. 24**, and the photovoltaic parameters of each are indicated in **Table 5**. The enhancement of photo-conversion efficiency by using AB process was confirmed by all the different electrolyte types.

When the photovoltaic parameters were compared with a DSSC using conventional liquid-type electrolyte, short-circuit current density of a DSSC using UV-cured polymer gel type electrolyte is lower, due to the low ionic mobility in a viscous medium at room temperature despite its merit of the long-term stability and rather higher photovoltaic performance at high temperature. However, the DSSCs using double layer gel type electrolyte with additional nano-gel type electrolyte on the UV-cured polymer gel type electrolyte have shown analogous level of photo-conversion efficiency to the DSSC using high performance liquid-type electrolyte with similar short-circuit current density and higher open circuit voltage while maintaining long-term stability of the UV-cured gel type electrolyte. This is

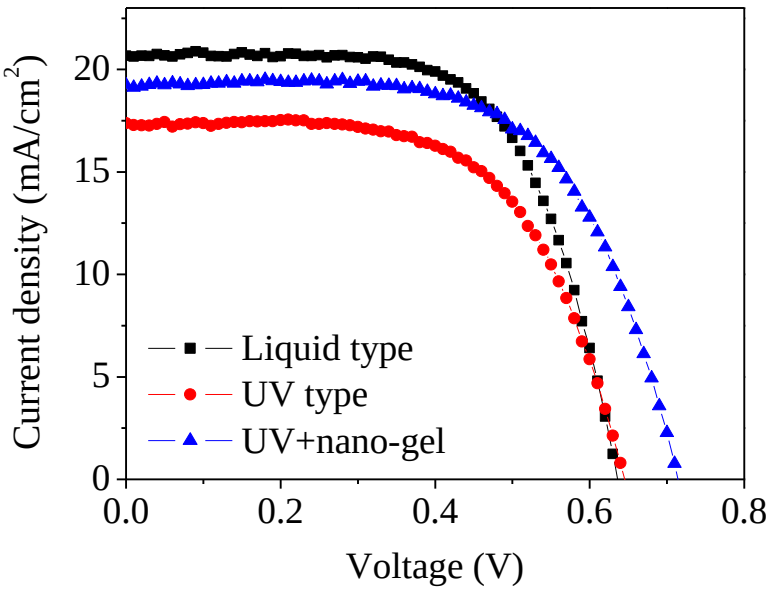

Fig. 25. Current density-voltage (*J–V*) curves of the DSSCs fabricated using different types of electrolytes as liquid-type, UV-cured polymer gel type, and double layer gel-type on the AB TiO_2 photo-anode films, measured by solar simulator under 1 sun, AM 1.5G condition.

Table 5. Photovoltaic parameters of the DSSCs fabricated using different types of electrolytes as liquid type, UV-cured polymer gel type, and double layer gel-type on the AB TiO2 films, and measured by solar simulator under 1 sun, AM 1.5G condition.

Electrolyte	**V_{OC} (V)**	**J_{SC} (mA/cm^2)**	**F/F (%)**	**η (%)**
Liquid type	0.636	20.7	65	8.49
UV type	0.645	17.4	62	6.92
UV + nano-gel	0.714	19.2	63	8.72

because of the improved charge transfer rate between the electrolyte and counter electrode although the thickness of the gel-type electrolyte has become even thicker.

Incident photon-to-current conversion efficiencies (IPCEs) were compared between the DSSCs with Normal films and AB films commonly using double layer gel-type electrolyte and the results are shown in **Fig. 26**. The IPCEs of the DSSCs using AB TiO_2 photo-anode films were increased in longer visible wavelength regions from 500 nm to 750 nm due to the effect of light recycling in the TiO_2 photo-anode films compared to the DSSCs using Normal TiO_2 photo-anode films without light scattering layer. This is a typical result indicating that the improved photo-conversion efficiency comes from light scattering effect and have a merit of utilization of longer visible wavelength regions.

The stability of the DSSCs incorporating the AB TiO_2 photo-anode film and a double layer gel-type electrolyte under continuous light illumination conditions were tested and the results are shown in **Fig. 27**. As a representative parameter indicating the long-term stability, photo-conversion efficiencies of the DSSCs using double layer gel-type electrolyte were maintained well until the end of 300 hours test. (Photovoltaic performances are shown in **Table 6.**)

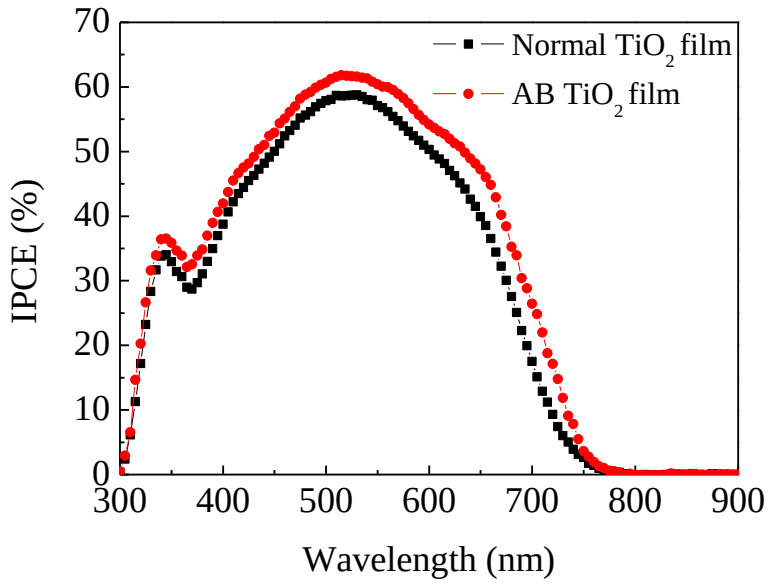

Fig. 26. Incident photon-to-current conversion efficiencies (IPCEs) measurement of the fully aged DSSCs using normal TiO_2 photo-anode films or AB TiO_2 photo-anode films commonly with double layer gel-type electrolyte.

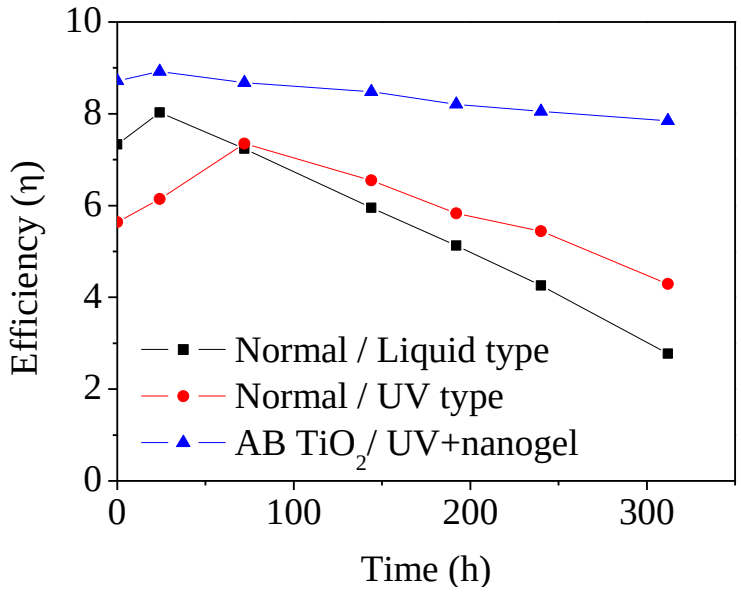

Fig. 27. Stability test result of the DSSC using double layer gel-type electrolyte with AB TiO_2 photo-anode film compared with DSSCs using Liquid type or UV type electrolyte with Normal TiO_2 photo-anode film measured by solar simulator under continuous light illumination at ambient temperature.

Table 6. Photovoltaic performances of the DSSCs with different TiO_2 films and electrolytes at light-soaking test.

TiO_2 film	**Electrolyte**	**0 hr**	**72 hr**	**192 hr**	**312 hr**
Normal	**Liquid**	7.33	7.24	5.13	2.77
	UV polymer	5.64	7.35	5.83	4.29
AB	**UV polymer + Nano-gel**	8.72	8.68	8.21	7.85

Initial photo-to-current conversion efficiency of DSSC using AB TiO_2 film and double layer gel type electrolyte was improved 18% and maintained 2.8 times higher photo-to-current conversion efficiency compared to the DSSC using normal TiO_2 film and liquid electrolyte. This result means that the contact between the TiO_2 films and the electrolytes were intimately maintained and sensitized dyes were not segregated until each measurement time.

3.4 Conclusions

In summary, we demonstrated the control of morphology and optical properties of the TiO_2 photo-anode films by simply adding high temperature volatile material in the TiO_2 paste without using cumbersome hard or soft template. As a result, the light scattering effect and the infiltration process of gel-type electrolyte could be improved.

We investigated for the optimal heat treatment condition in which complete evaporation of AB was facilitated for the formation of micro-crater structure, and improved the optical properties such as opacity, haze and whiteness index values. On the contrary, the excess heat treatment condition resulted in the shrinkage of micro-porous morphology. In this study, the performance of the DSSCs with double layer gel-type electrolyte was enhanced to the level of 8.7 % from 7.9 % by using AB TiO_2 film through the optimization of optical properties without using any additional light scattering layer.

Furthermore, the facile process of electrolyte infiltration by this method is considered to be a great prospect for large scale commercialization of quasi-solid state DSSCs in the near future.

Chapter 4. Outdoor stability

4.1 Current methods

In case the TiO_2 nanoparticles coated on the photo-anode absorb a UV light, they act as a photocatalyst inducing the degradation of sensitizing dye.[52] It was demonstrated by measuring the photo emission spectra of activated DSSCs that chemisorbed dye molecules are oxidized by the high-energy holes photogenerated in the valence band of TiO_2 under UV irradiation. In case the water content is high in the DSSC, the sensitizer can degrade and desorb from TiO_2 surface with the synergy of water and UV light.

Also, the tri-iodides (I_3^-) in liquid electrolyte, which act as a redox couple with iodide (I^-), are reduced irreversibly on the TiO_2 surface to colorless iodide ions by the photocatalyst effect, followed by inducing a lack of reversible oxidation-reduction reaction of the electrolyte.[53] The decrease of I_3^- concentration (i) increases the series resistance which leads to a lower fill factor, (ii) limit the short circuit current density because of mass transport limitations, and (iii) by-product of the bleaching reactions increases the back recombination rates. In this reason, DSSCs need a UV cut-off filter for the protection

of degradation by UV light. Major commercial PET-based UV cut-off filters are λ_{320}, λ_{385}, λ_{420} and λ_{480}, which cut-off each level of UV lights, respectively.

DSSCs without UV cut-off filter show higher photo-to-current conversion efficiencies but lower stability at outdoor conditions. On the contrary, DSSCs with UV cut-off filter have higher stability at outdoor conditions but lower photo-to-current conversion efficiency due to large amount of incident light loss.[54] UV cut-off materials are selected among UV absorbing materials like as silica, alumina, zirconia, titania and ceria to cut off wavelength under 387 nm selectively, which is the maxima absorption peak of anatase type TiO_2.[55]

However, there has been limit to mitigate the relative drop of photo-conversion efficiency using conventional UV cut-off filter only, because the filtered amount of UV light cannot be re-used for DSSCs operation.[56]

There are two principal approaches to utilize UV light efficiently. First approach is to improve electronic properties of first/second generation cell by very narrow junction, low doping level, and very thin window layers, and to improve electronic properties of third generation cell by multijunction, heterojunction, and intermediate

band gap. Second approach is to use spectrum conversion layer incorporating host materials of polymers, inorganic crystalline materials, glass, and organic molecule silicates, and luminescent materials of quantum dots, organic dyes and rare-earth ions/complexes. However, improving the electronic properties of existing devices are difficult to implement.

Spectrum conversion design for PV applications involves down-shifting (DS), quantum-cutting (QC), and upconversion (UC). The DS and QC materials are usually placed on the front surface, whereas, UC materials are placed on the light-reflector layer. Solar cell device equipped with a luminescent solar concentrator and reflection mirror guides the emitted light to solar cells placed next to the edge of the slab. On the contrary, solar cell device with a luminescent down-shifting layer directly placed onto the surface of the solar cell exhibits a better spectral response by absorbing short wavelength photons and then re-emitting them at a longer wavelength. However, there was a challenge finding optimal host material and luminescent species to block whole UV light while emitting longer enough wavelength for power generation.

4.2 New fabrication method

To address this issue, we propose a novel system using unique combination of SCL materials with UV absorbing 1,8-naphthalimide derivatives on the photo-anode. There have been advanced researches to enhance the photo-to-current conversion efficiency of DSSCs using (i) quantum dots (ii) organic dyes[57] and (iii) rare-earth ions/complexes as spectrum conversion materials by (i) coating on the front or rear glass (ii) doping into the TiO_2 nanoparticles and (iii) dispersing in the liquid electrolyte.[58]

However, there was little improvement of photo-to-current conversion efficiency through coating spectrum conversion materials on the front glass against previous theoretical expectations.[59] Meanwhile, applying the spectrum conversion materials by dispersing in the liquid electrolyte or by coating on the rear glass were more effective to improve the photo-conversion efficiency.[60] This result arises from the large loss of incident light and deficient utilization of absorbed light, because the emitted wavelength from spectrum conversion layer (SCL) is too short to be used by the sensitizing dye.[61] The spectrum range needed to shield for outdoor stability is under 387 nm and the spectrum range needed to enhance the photo-to-

current conversion efficiency is a visible light between 400 and 530 nm. Thus, the challenge of replacing UV cut-off filter with SCL for outdoor stability is to increasing the stoke shift large enough for effective utilization by sensitizing dye.[62]

To increase the stoke shift by the formation of dimeric complex molecule upon UV absorption, we used a heteromolecular compound of 1,8-naphthalimide derivatives. A compound of 1,8-naphthalimide derivatives as a guest material and poly (ethylene-co-vinyl acetate) as a host material was dissolved in toluene solvent to form a functional layer on the photo-anode of the DSSC. (see **Fig. 28**) Prepared 1,8-naphthalimide derivatives are generally synthesized from the corresponding anhydrides by reaction with alkyl amine. Each alkyl amine with different alkyl chain produces different family of derivatives showing unique fluorescent properties. General synthetic route for 1,8-naphthalimide derivatives, numbering and representative formula are shown in **Fig. 29.**

To demonstrate the effect of SCL with heteromolecular fluorescent compound, we conducted several analyses as follows. First, we have shown that the stokes shift could be increased by the formation of dimeric complex at higher concentration of the 1,8-naphthalimide derivatives, by measuring the transmittance,

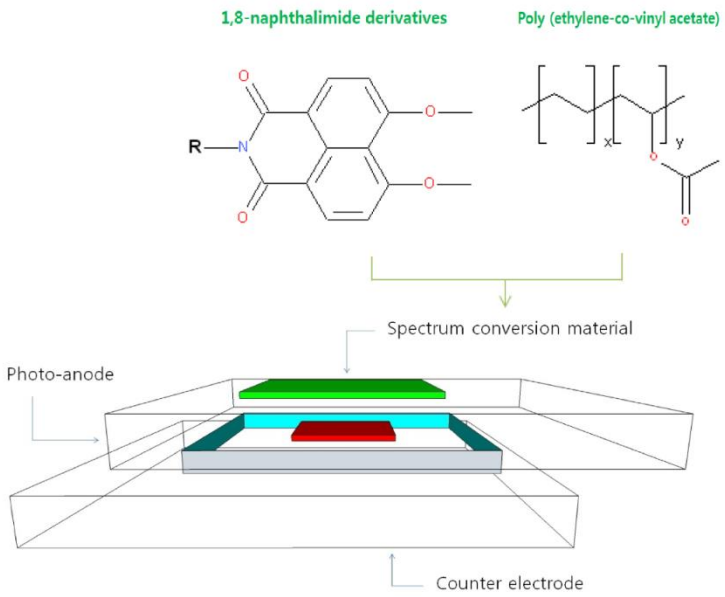

Fig. 28. Dimer complex forming spectrum conversion material with a compound of 1,8-naphthalimide derivatives in EVA (poly (ethylene-co-vinyl acetate)) is coated on the photo-anode of the DSSC.

(a)

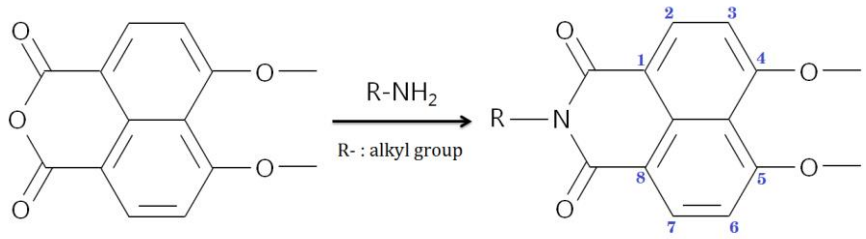

(b)

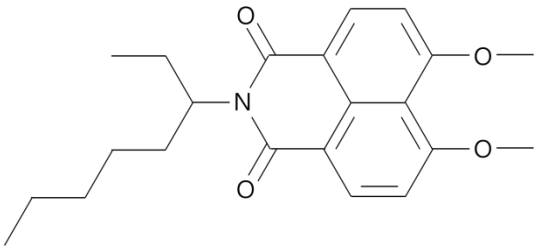

Fig. 29. (a) General synthetic route and numbering (b) representative formula of 1,8-naphthalimide derivatives; Family of derivatives are synthesized by the reaction of 1,8-naphthalic anhydride (6,7-dimethoxy-benz[*de*]isoquinolin-1,3-dione) with kinds of alkyl amines. Representative formula is (2-(1-ethylhexyl)-6,7-dimethoxy-benz[*de*]isoquinolin-1,3-dione), CAS No. 139106-96-0, Molecular Formula $C_{22}N_{27}NO_4$ and Molecular Weight 369.45 g/mole

absorbance, and fluorescence of the SCL on the FTO glass. Second, the evidence of converting absorbed UV light for power generation in DSSC by SCL was shown by measuring the IPCE especially under 370 nm and photo-to-current conversion efficiency of the prepared DSSCs. Finally, we conducted outdoor stability test using prepared DSSCs for 48 days at outdoor field. As a result, DSSC with SCL has shown comparable initial photo-conversion efficiency to bare DSSC and maintained 18% higher relative photo-to-current conversion efficiency after 48 days outdoor condition than DSSC using commercial UV cut-off filter.

(A) Preparation of Spectrum Conversion Material

A compound of 1,8-naphthalimide derivatives as a spectrum conversion material was prepared from a company (Lumicolor-Violet, ICB Korea). Poly (ethylene-co-vinyl acetate) (EVA, vinyl acetate 40 wt.%, Aldrich) bead 5 wt.% was dissolved in toluene as a host material stock solution. Different concentrations of spectrum conversion materials were prepared by dissolving 1,8-naphthalimide derivatives in host material stock solution with the ratios of 0.5, 1.0, 1.5, 2.0, 2.5 and 3.0 wt.% respectively. TiO_2 sol (solution of TiO2 nanoparticle diameter 15nm, ENB Korea) was prepared as a reference UV absorbing material. Commercial UV cut-off film (PR70, 3M) was prepared as a reference UV cut-off filter.

(B) Fabrication of the DSSC

Photo-anode films were prepared by screen printing TiO_2 pastes on the FTO glass (TEC 8/2.3mm, 8 Ω/sq, Pilkington) with aperture area of 0.2 cm^2 and sintered at 550 ℃ for 30 min. Dye adsorption was carried out by dipping the TiO_2 photo-anode films into a 4×10^{-4} M t-butanol/acetonitrile (Merck, 1:1) solution of the ruthenium dye (N719, Solaronix) for 48 hour at 25 ℃. Nano-gel type electrolyte which was prepared according to the previously reported method adding silica nanoparticle was coated on the TiO_2 photo-anode film. Counter electrodes were prepared by dropping of 10 mM hydrogen hexachloroplatinate (IV) hydrate (99.9%, Aldrich) in a 2-propanol solution onto the transparent FTO glass and after treatment at 400 ℃ for 30 min. The two electrodes were assembled and separated using thermal adhesive polymer film (Surlyn, thickness 60 ㎛).

(C) Formation of Spectrum Conversion Layer

FTO glasses (25 mm x 40 mm) were prepared by washing and sonication. Each side of the FTO glasses or DSSCs was masked using polyimide tape before coating 1,8-naphthalimide derivatives on the FTO glass using dip coater, to open the active area of front side only. Prepared FTO glasses or fabricated DCCSs were dipped in 1,8-naphthalimide derivatives solution to form dimeric complex forming SCL on the substrate using table-top dip coater (e-flex, EF-4200). The raising speed of the dip coater was controlled between 1 and 10 mm/sec after dipping 5 seconds in solution to keep the optimal thickness for anti-reflection.

(D) Characterization of the SCL and DSSC

In order to investigate the optical properties of SCL, transmittance and diffuse reflectance of the FTO glasses with SCL were measured using UV-vis spectrophotometer (CM-5 Konica Minolta, Japan) and analyzed with color data software (SpectraMagic NX Ver.2.1 Konica Minolta, Japan). The absorbance of the SCL was calculated from the obtained transmittance and reflectance data. The fluorescence of the SCL was evaluated by measuring the emission spectrum of the FTO glasses with SCL using Fluorescence Spectrometer (FS-2, scinco) and analyzing with spectrum data software (FluoroMaster Plus Software, Scinco). Emitted photon numbers between the wavelength of 300 and 700 nanometers by the excitation at 370 nanometer UV light were counted by the probe under fixed condition of scan speed 300 nm/min and PMT voltage 500 volt followed by spectrum correction.

(E) Characterization of the photovoltaic properties

The photovoltaic properties of the prepared DSSCs were measured using a 1600W Ozone free lamp with a ‘Class A’ Air Mass 1.5G filter as a light source in a solar simulator (Newport-94083A) and with an exposure control instrument (Newport-68951). The light intensity was adjusted with a reference Si cell (Fraunhofer Institute for Solar Energy System). Photovoltaic performance was characterized by *Voc*, *Jsc*, and *FF* (fill factor), and the overall photo-to-current conversion efficiency was characterized using the current density-voltage (*J*-*V*) curve.

Incident photon-to-current conversion efficiencies (IPCE) were measured by the illumination of prepared DSSC with a 200W Xenon Arc light source through a filter monochromator using optical chopper rotating at 2 Hz under 1 sun bias light (Newport-CS260).

For the test of outdoor stability under continuous UV light irradiation, the prepared DSSCs were arrayed on an outdoor field which was set up custom-built for this study. Then, the photo-to-current conversion efficiencies were characterized weekly.

4.3 Properties and stability

Transmittance of the FTO glass coated with TiO_2 sol was measured as a reference UV absorbing material. **Fig. 30** shows that the transmittance of the FTO glass coated with TiO_2 sol was cut off below 370 nm compared to that of bare FTO glass. UV cut-off peak was slightly red shifted according to the number of dip coating, though the change was very little. This UV cut-off is needed because the degradation of DSSC by UV light occurs as a result of photocatalytic reaction from the direct excitation of the TiO_2 band gap. Anatase phase TiO_2 is photoactive up to 387 nm with band gap of 3.2 eV, while rutile phase TiO_2 is photoactive up to 411 nm with band gap of 3.02 eV. If the photo-anode is made with TiO_2 nanoparticle starting from a mixture of anatase and rutile phase (for example, Degussa P25), the UV cut-off filter must shield up to 411 nm. However, if the whole incident UV light under 411 nm were cut-off without re-using, relative drop of photo-conversion efficiency would be large compared to the bare DSSC without UV cut-off filter.

Transmittance of the FTO glass coated with 1,8-naphthalimide derivatives for SCL was measured according to the concentrations to show the possibility as a substitute for UV cut-off filter. **Fig. 31** shows

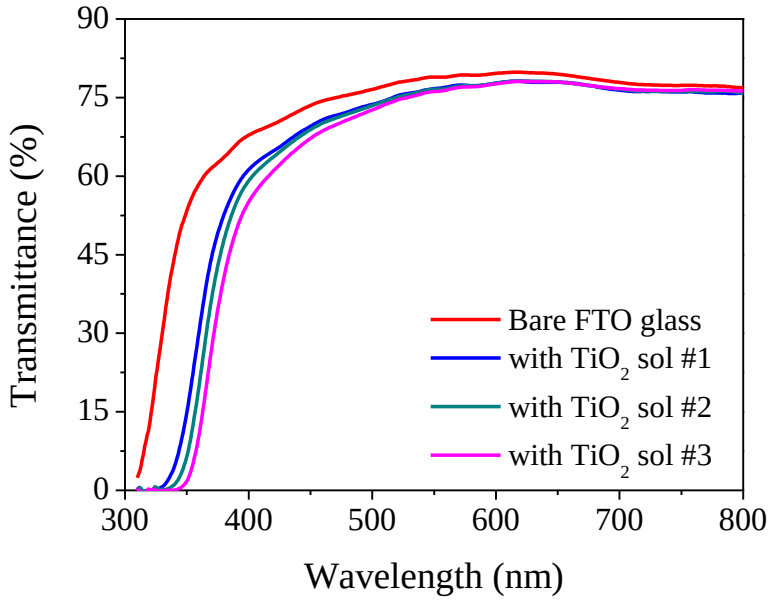

Fig. 30. Transmittances of TiO_2 sol coated FTO glasses;
TiO_2 sol was coated 1, 2 and 3 times on FTO glasses as a reference UV absorbing materials, corresponding to TiO_2 sol #1, #2 and #3, respectively.

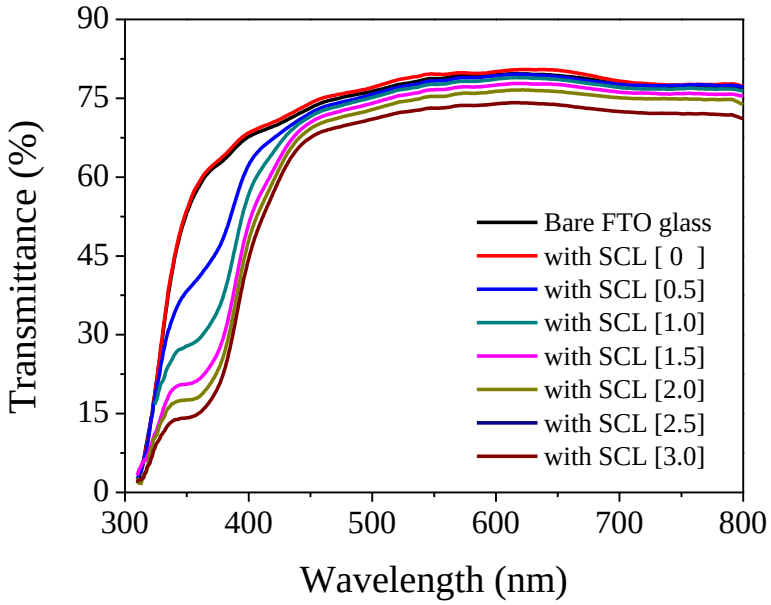

Fig. 31. Transmittances of FTO glasses with SCL of 0, 0.5, 1.0, 1.5, 2.0, 2.5 and 3.0 wt.% 1,8-naphthalimide derivatives, respectively.

that the transmittance of the SCL below 370 nm falls down according to the concentration of the 1,8-naphthalimide derivatives. Additionally, the absorption edge was red shifted gradually up to 400 nanometers. However, the visible light transmittance decreased slightly according to the concentration of the 1,8-naphthalimide derivatives. The concentration of 1,8-naphthalimide derivatives over 2 wt.% was favorable for higher UV light stability, but, further gain of UV light stability according to the concentration was very small while the loss of light transmission increased. To maintain a balance between UV light stability and photo-conversion efficiency, higher outdoor performance was expected at the concentration of 2 wt.% of 1,8-naphthalimide derivatives, showing high absorbance at UV absorption peak and wide range of absorption edge to cover the absorption range of TiO_2 film on the photo-anode, previously.

The absorbance of the coating layers were calculated from the measured transmittance and reflectance data. (The reflectance curve is shown in **Fig. 32**) **Fig. 33** shows that the absorption peak is at around 370 nm and absorption edge is at around 414 nm for SCL. The absorption peak of TiO_2 sol coated FTO glass as a reference material for UV absorbing property of the photo-anode shows the similar shaped graph with SCL coated FTO glass. This result confirms that

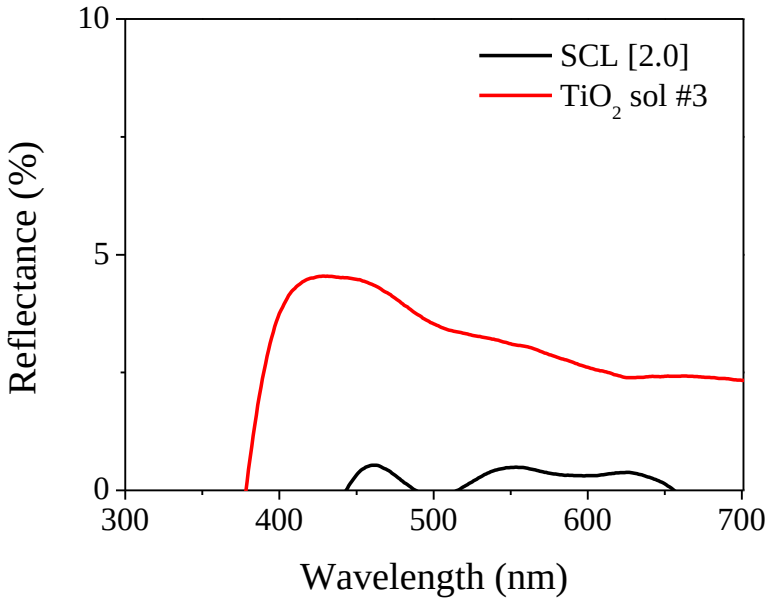

Fig. 32. Reflectances of SCL and TiO_2 sol coated FTO glasses;
The concentration of 1,8-naphthalimide derivatives was 2 wt.% for SCL [2.0] and the number TiO_2 sol coating was 3 times for TiO_2 sol #3.

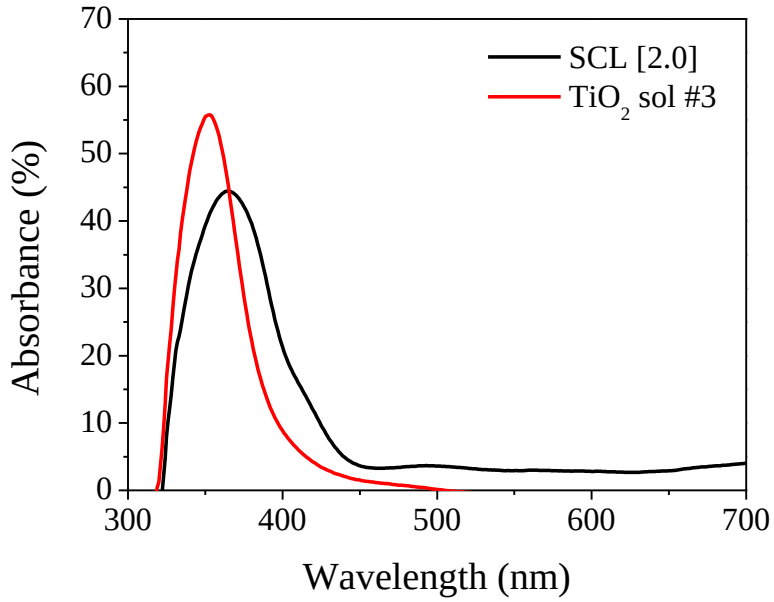

Fig. 33. Absorbances of SCL and TiO_2 sol coated FTO glasses;
The concentration of 1,8-naphthalimide derivatives was 2 wt.% for SCL [2.0] and the number TiO_2 sol coating was 3 times for TiO_2 sol #3. Absorbances were calculated from the transmittance and reflectance.

absorption peak of SCL is adequate to cover the absorption peak of photo-anode and the absorption band is adequate to block the required range of UV light to replace the UV cut-off filter, which shields the UV light on the TiO_2 nanoparticulate photo-anode film layer.

Fluorescence of the SCL by the excitation at 370 nm was measured with prepared SCL FTO glasses using 1,8-naphthalimide derivatives with concentration of 0, 0.5, 1.0, 1.5, 2.0, 2.5 and 3.0 wt.%, respectively. **Fig. 34** shows that the emission peak of SCL remained at 424 nm under low concentration, however, the peak was gradually red shifted up to 476 nm by increasing the concentration of 1,8-naphthalimide derivatives to 2 wt.%, thereafter, it was saturated at further increase of concentrations. Therefore, stokes shift moved from 54 nm to 106 nm at 2 wt.% 1,8-naphthalimide derivatives due to the formation of dimers. The fluorescence profiles of SCM(1) and SCM(2) at the same concentration in dimethylformamide (DMF) solvent are shown in **Fig. 35**. This phenomenon can be explained by the formation of dimeric complex molecules at high concentration in the excited state. Because, dimeric complex molecule formation is dependent on a bimolecular interaction, it is promoted by high monomer density. At low density, excited monomers decay to the ground state before they interact with an unexcited monomer to form dimeric complex

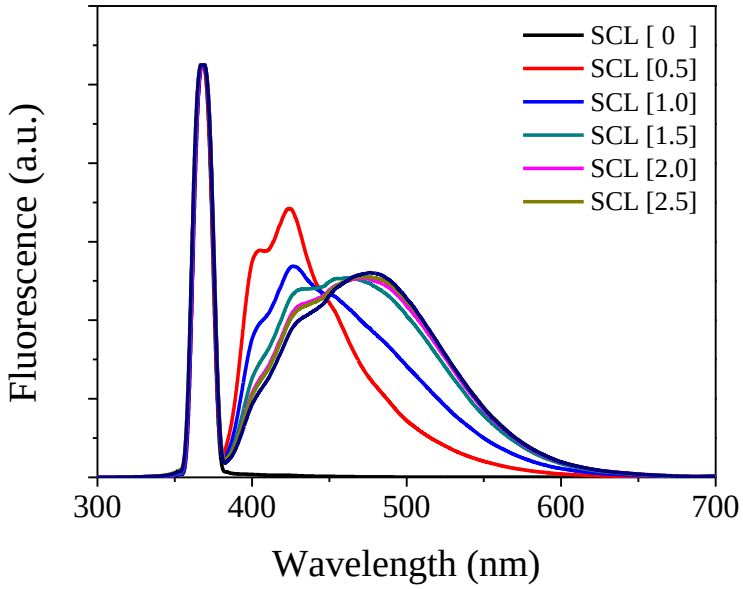

Fig. 34. Fluorescences of FTO glasses with SCL of 0, 0.5, 1.0, 1.5, 2.0, 2.5 and 3.0 wt.% 1,8-naphthalimide derivatives, respectively.

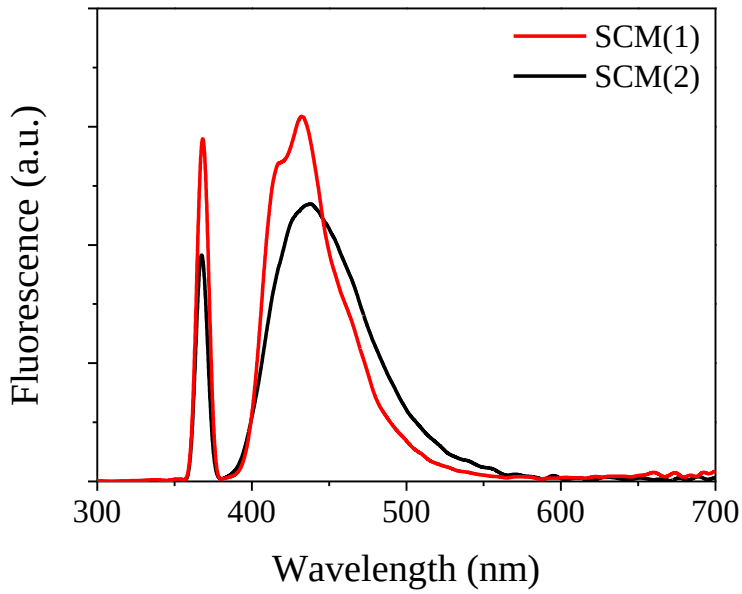

Fig. 35. The fluorescence of SCM(1) and SCM(2) in DMF solvent.

molecule. However, at high density, formation of dimeric molecule is possible very shortly on the order of nanoseconds in an electronic excited state. Once one of the heterodimer components is excited by the absorption of UV light, the charge is transferred to the LUMO (Lowest Unoccupied Molecular Orbital) of unexcited component monomer followed by emitting longer wavelength light with smaller energy.[63]

Traditional N719 dye has shown high photo-conversion efficiency exceeding 11 % when employing I^-/I_3^- liquid electrolyte, despite relatively intense absorptions between 400 and 535 nm ($\varepsilon \approx$ 14000 $M^{-1}cm^{-1}$), due to high open circuit potential and ultrafast electron injection after light absorption. The absorption maximum for N719 dye bound to TiO_2 is 531 nm (2.34 eV), having a lowest optically active excited state from the dye π^* located at 0.3 eV above the lowest transition localized in the TiO_2. By the formation of dimeric complex molecule, the emission spectrum of SCL could reach to the lowest optically active excited state of N719 dye bound to TiO_2 to produce higher energy for the minimum driving force needed for electron injection.[64]

The thickness of SCL after dip coating is a very important figure for optic and economic valuation of proposed system. The thickness of

SCL with 0 wt.% of 1,8-naphthalimide derivatives was identified to be between 253 ~ 263 nanometers using scanning electron microscope (SEM). The thicknesses of SCL containing 1,8-naphthalimide derivatives were kept to be same with SCL with 0 wt.% to keep optimal optic property. **Fig. 36** shows the cross-section picture of SCL with 0 wt.% 1,8-naphthalimide derivatives on FTO glass taken by SEM after pretreatment with liquid nitrogen for rapid cooling. However, further cross-section measurement was difficult by the elasticity of the SCL.

To investigate the initial photo-to-current conversion efficiency drop by the additional layer on the DSSC, the DSSCs were prepared using TiO_2 nanoparticulate film of anatase/rutile phase mixture, N719 sensitizing dye and nano-gel type electrolyte with I^-/I_3^- redox couple. **Fig. 37** shows the photo-to-current conversion efficiency result of the DSSCs having bare, SCL and UV cut-off filter coated FTO glasses, respectively. Relative photo-conversion efficiency of DSSC using commercial UV cut-off filter dropped 22.6 % compared to the bare DSSC. On the contrary, the relative photo-to-current conversion efficiency DSSC using SCL was 0.07 % higher compared to the bare DSSC by the effect of anti-reflection effect and conversion of absorbed UV light, despite the large loss of visible light source due to

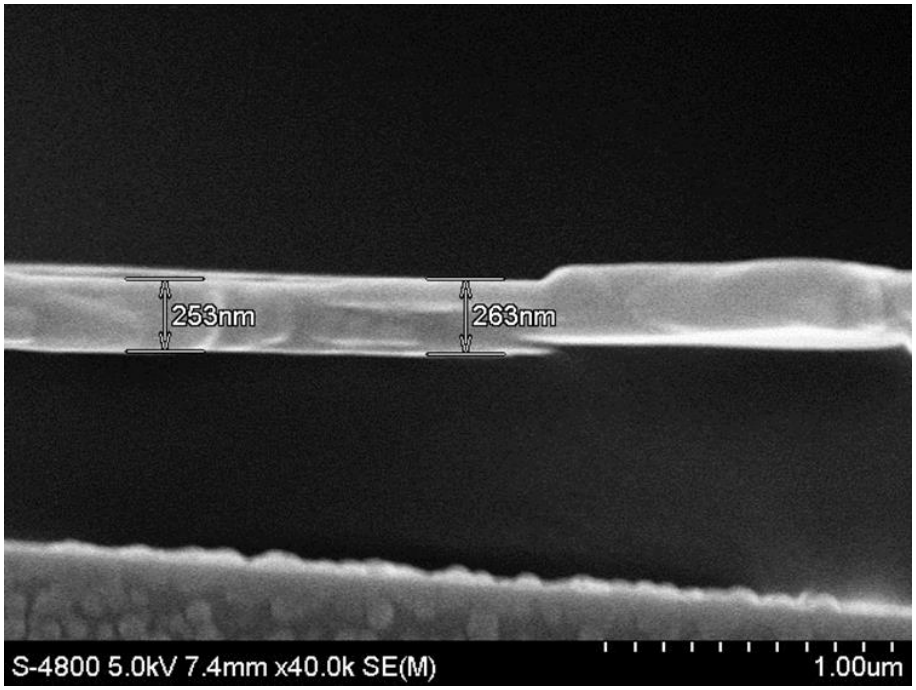

Fig. 36. Cross-section of SCL coated on the FTO glass by scanning electron microscope (SEM) after pretreatment using liquid nitrogen for rapid cooling.

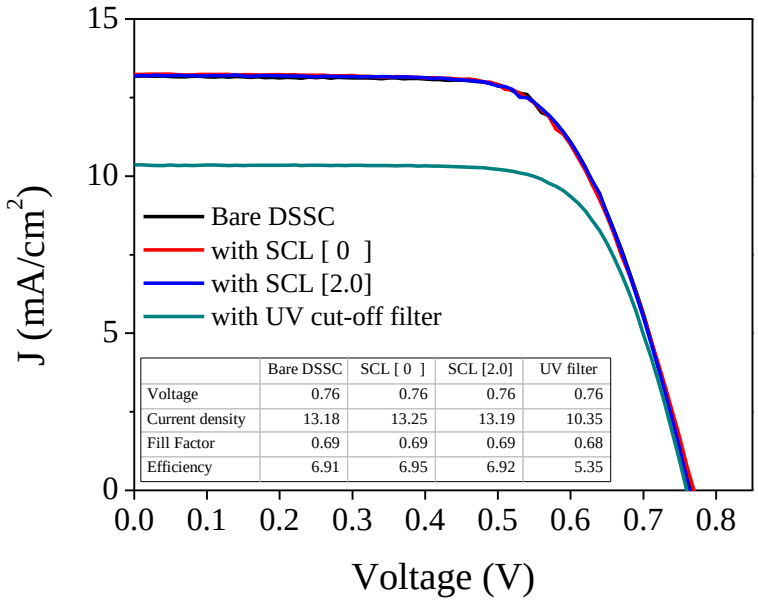

	Bare DSSC	SCL [0]	SCL [2.0]	UV filter
Voltage	0.76	0.76	0.76	0.76
Current density	13.18	13.25	13.19	10.35
Fill Factor	0.69	0.69	0.69	0.68
Efficiency	6.91	6.95	6.92	5.35

Fig. 37. Initial photo-to-current conversion efficiencies of the prepared DSSCs using (i) bare FTO glass without any optical filter, (ii) 1,8-naphthaimide derivatives 0 and 2 wt.% as SCL and (iii) commercial UV cut-off filter, respectively.

longer wavelength absorption edge. **Fig. 38** shows the transmittance and reflectance of commercial UV cut-off filter. Total transmittance was 69.5 % and UV cut-off edge was 400 nm. **Fig. 39** shows the difference of photo-to-current conversion efficiency of DSSCs with SCL 2 wt.% and bare DSSC. Number of sample was 37 and the maximum deference was below 0.3 %.

To demonstrate more concrete evidence to prove the enlarged usage of incident UV light, Incident Photon-to-Current conversion efficiencies (IPCE) of the prepared DSSCs were compared. **Fig. 40** shows the IPCE result of the DSSCs having bare, SCL and UV cut-off filter coated FTO glass, respectively. There was a very interesting finding in the IPCE result of DSSC using SCL at UV range below 370 nm. The IPCE value of DSSC using SCL was 19 % at 370 nm, this efficiency is extraordinarily high. The IPCE value of DSSC using bare FTO glass was 36 % from the transmittance of 61 % at the same wavelength. The expected IPCE value from the transmittance of 21% is only 12 %, in case of DSSC using SCL. Therefore, there was an extra gain of 7 % IPCE value at 370 nm. This is a compelling evidence of re-using absorbed UV light to achieve prominent photo-conversion efficiency enhancement by the spectrum conversion.

As an ultimate objective of this study, outdoor photo-to-current

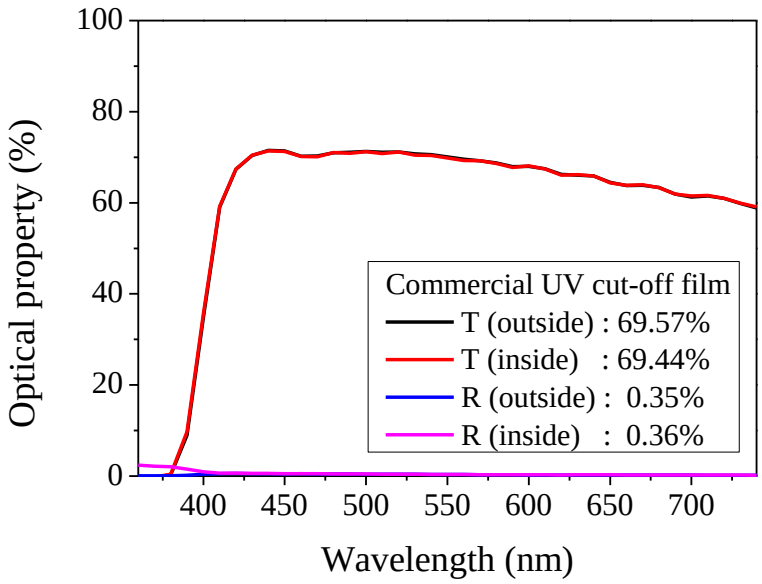

Fig. 38. Transmittance and reflectance of commercial UV cut-off filer;

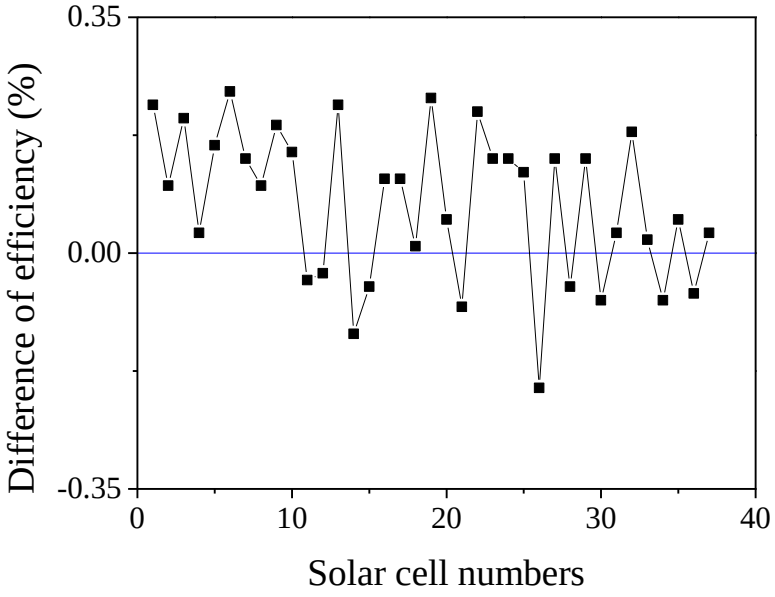

Fig. 39. Difference of photo-to-current conversion efficiency of DSSCs with SCL and bare DSSC. The concentration of 1,8-naphthalimide derivatives was 2 wt.%.

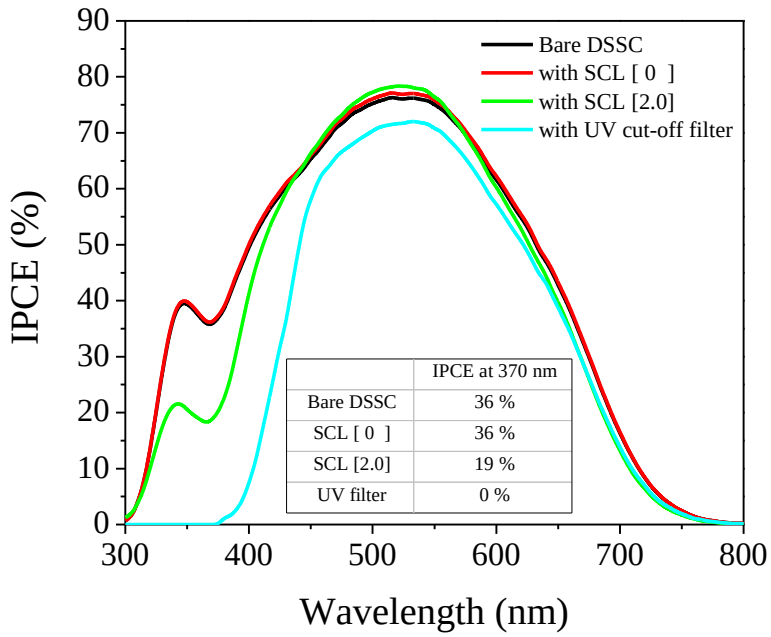

Fig. 40. Incident Photon-to-Current conversion efficiencies (IPCE) of the prepared DSSCs using (i) bare FTO glass without any optical filter, (ii) 1,8-naphthaimide derivatives 0 and 2 wt.% as SCL and (iii) commercial UV cut-off filter, respectively.

conversion efficiencies of the prepared DSSCs were compared. **Fig. 41** shows the relative outdoor photo-to-current conversion efficiency result of the DSSC using bare, SCL and UV cut-off filter, respectively. (see **Table 7**. for numeric relative performance data) Relative photo-to-current conversion efficiency (PCE) of bare DSSC decreased to 76%. DSSC with SCL [0] showed slightly higher PCE due to anti-reflection effect. using a compound of 1,8-naphthalimide derivatives for SCL maintained to 87% due to spectrum conversion and it was 18% higher than the DSSC using commercial UV cut-off filter, after 48 days outdoor conditions, which confirms that the higher performance was achieved at outdoor condition by the additional dimeric complex forming SCL coated on the bare DSSC.

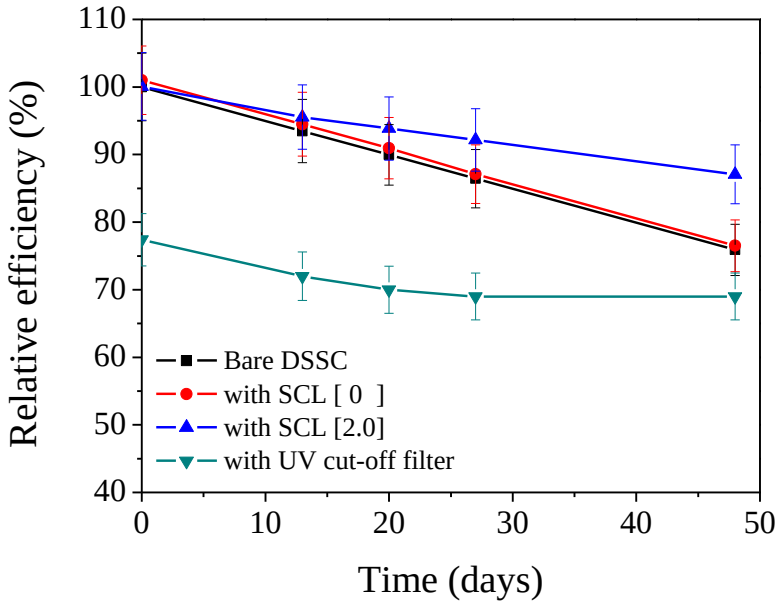

Fig. 41. Relative outdoor photo-to-current conversion efficiencies of the prepared DSSCs using (i) bare FTO glass without any optical filter, (ii) 1,8-naphthaimide derivatives 0 and 2 wt.% as SCL and (iii) commercial UV cut-off filter, respectively.

Table 7. Relative outdoor photovoltaic performances of the prepared DSSCs using (i) bare FTO glass without any optical filter, (ii) 1,8-naphthaimide derivatives 0 and 2 wt.% as SCL and (iii) commercial UV cut-off filter, respectively.

	0 d	**13 d**	**20 d**	**27 d**	**48 d**
Bare DSSC	100	93	90	86	76
with SCL [0]	101	94	91	87	77
with SCL [2.0]	100	96	94	92	87
with UV filter	77	72	70	69	69

4.4 Conclusions

In summary, the potential of unique combination of SCL materials with UV absorbing 1,8-naphthalimide derivatives as a substitute to the UV cut-off filter on the DSSC was studied to enhance the outdoor stability. The measurement of transmittance and absorbance of SCL coated FTO glass showed that the UV light below 414 nm could be largely absorbed. The measurement of Stokes fluorescence of SCL coated FTO glass showed that the emission peak could be red shifted from 424 nm to 476 nm at 2 wt.% concentration of a compound of 1,8-naphthalimide derivatives according to the formation of dimeric complex molecules upon UV absorption. The Incident Photon-to-Current conversion efficiency result provided concrete evidence that the absorbed UV light below 370 nm was converted into a longer wavelength and used to enhance the photo-to-current conversion efficiency. The actual outdoor field test was conducted to evaluate the ultimate objective of the DSSC using proposed spectrum conversion layer with a compound of 1,8-naphthaimide derivatives. Outdoor stability test for 48 days demonstrated that the functional layer coated on the DSSC with concentration of 1,8-naphthalimide derivatives 2 wt.% helped to

maintain the comparable initial photo-to-current conversion efficiency and 18% higher relative photo-conversion efficiency after 48 days than DSSC using commercial UV cut-off filter. We believe that our new finding would provide inspiration to enhance outdoor stability of DSSCs especially for building and automobile integrated photovoltaic devices.

Chapter 5. Conclusions

Two fabrication methods have been developed for enhanced stability of Dye-sensitized solar cells (DSSCs) : double layer gel-type electrolyte and dimeric complex forming spectrum conversion layer. One fabrication method has been tailored for facile process of quasi-solid state electrolyte DSSCs : micro-crater structure of photo-anode.

The key element for long-term stability is the choice of sensitizing dye, electrolyte and UV cut-off filter, especially for outdoor condition. Ruthenium complex dye (N719) has been widely used due to high photo-conversion efficiency and proved stability. However, there has been contradiction between photo-conversion efficiency and long-term stability in electrolyte and UV cut-off filter.

To enhance the photo-conversion efficiency of long-term stable UV-cured polymer gel electrolyte, additional nano-gel electrolyte layer was introduced between the above-mentioned electrolyte and counter electrode. Resultant double layer gel type electrolyte showed a lower charge transfer resistance due to the increase of exchange-reaction-based charge diffusion effect despite the influence from increase of electrolyte thickness.

The crucial factor using quasi-solid state electrolyte is decreasing

contact resistance between TiO_2 nanoparticle film and electrolyte. To accomplish fast and complete electrolyte infiltration into the TiO_2 nanoparticle film, micro-crater structure was formed using acetylene-black as an evaporated material at high temperature. This morphology improved light scattering effect without using additional layer.

Although TiO_2 film facilitates an essential structure for photo-anode, decreases the outdoor stability of DSSCs by absorbing UV light to degrade sensitizing dye and redox couple. To convert damaging UV light into longer wavelength light in advance, additional spectrum conversion layer was introduced on the photo-anode. Similar structured two spectrum conversion materials formed dimeric complex at high concentration to increase the stoke shift.

In this research, three new methods were developed using conventional DSSCs to avoid unexpected influence from environment. However, these new techniques are useful for the next generation solar cells regardless of the kind or shape of the device to improve the long-term stability while maintaining high photo-to-current conversion efficiency.

Notation

I_{inj}	charge flux from dye sensitized injection, Eqs. (1)
n_{cb}	surface electron concentration at the TiO_2 surface, Eqs. (1)
k_{ct}	the rate constant of the I_3^- reduction reaction, Eqs. (1)
D_{app}	apparent diffusion coefficient, Eqs. (2)
D_{phys}	physical diffusion coefficient, Eqs. (2)
D_{ex}	exchange-reaction-based diffusion coefficient, Eqs. (2)
k_{ex}	the exchange-reaction rate constant, Eqs. (2)
δ	center-to-center intersite distance, Eqs. (2)
c	concentration of the redox couple, Eqs. (2)
x	distance of the light, Eqs. (3)
(x)	intensity of light, Eqs. (3)
I_0	initial intensity of light, at x=0, Eqs. (3)
wt.%	weight percent

References

[1] A. Kay, M. Grätzel, *J. Phys. Chem.* **1993**, *97*, 6272-6277.

[2] J. J. Lagref, M. K. Nazeeruddin, M. Grätzel, *Inorganica Chimica Acta* **2008**, *361*, 735-745.

[3] (a) M.K.Nazeeruddin, A.Kay, I.Rodicio, R.Humphry-Baker, E.Muller, P.Liska, N.Vlachopoulos, M.Grätzel, *J. Am. Chem. Soc.* **1993**, *115*, 6382-6390; (b) M. K. Nazeeruddin, S. M. Zakeeruddin, R. Humphry-Baker, M. Jirousek, P.Liska, N.Vlachopoulos, V. Shklover, C.-H. Fisher, M. Grätzel, *Inorg. Chem.* **1999**, *38*, 6298-6305.

[4] T. Horiuchi, H. Miura, K. Sumioka, S. Uchida, *J. Am. Chem. Soc.* **2004**, *126*, 12218-12219.

[5] W. M. Campbell, K. W. Jolley, P. Wagner, K. Wagner, P. J. Walsh, K. C. Gordon, L. Schmidt-Mende, M. K. Nazeeruddin, Q. Wang, M. Grätzel, D. L. Officer, *The Journal of Physical Chemistry C* **2007**, *111*, 11760-11762.

[6] M. Grätzel, *Acc. Chem. Res.* **2009**, *42*, 1788-1798.

[7] H. Zhou, L. Wu, Y. Gao, T. Ma, *Journal of Photochemistry and Photobiology A: Chemistry* **2011**, *219*, 188-194.

[8] S. Ahmad, E. Guillén, L. Kavan, M. Grätzel, M. K. Nazeeruddin, *Energy & Environmental Science* **2013**, *6*, 3439-3466.

[9] C.-H. M. Chuang, P. R. Brown, V. Bulovic, M. G. Bawendi, *Nat. Mater.* **2015**, *13*, 796-801.

[10] Z. Pan, I. Mora-Sero, Q. Shen, H. Zhang, Y. Li, K. Zhao, J. Wang, X. Zhong, J. Bisquert, *J. Am. Chem. Soc.* **2014**, *136*, 9203-9210.

[11] M. Grätzel, *Nat. Mater.* **2014**, *13*, 838-842.

[12]N. J. Jeon, J. H. Noh, W. S. Yang, Y. C. Kim, S. Ryu, J. Seo, S. I. Seok, *Nature* **2015**, *517*, 476-480.

[13] B. O'Regan, M. Grätzel, *Nature* **1991**, *353*, 737-739.

[14] L. M. Gonçalves, V. de Zea Bermudez, H. A. Ribeiro, A. M. Mendes, *Energy & Environmental Science* **2008**, *1*, 655-667.

[15] S. Mathew, A. Yella, P. Gao, R. Humphry-Baker, B. F. E. Curchod, N. Ashari-Astani, I. Tavernelli, U. Rothlisberger, M. K.

Nazeeruddin, M. Grätzel, *Nature Chemistry* **2014**, *6*, 242-247.

[16] M. A. Green, K. Emery, Y. Hishikawa, W. Warta, E. D. Dunlop, *Progress in Photovoltaics: Research and Applications* **2014**, *22*, 701-710.

[17] T. M. Brown, F. D. Rossi, F. D. Giacomo, G. Mincuzzi, V. Zardetto, A. Reale, A. D. Carlo, *J. Mater. Chem. A* **2014**, *2*, 10788-10817.

[18] G. P. Lau, H. N. Tsao, S. M. Zakeeruddin, M. Grätzel, P. J. Dyson, *ACS Appl. Mater. Interfaces.* **2014**, *6*, 13571-13577.

[19] S. Ito, K. Takahashi, S.-i. Yusa, M. Saito, T. Shigetomi, *International Journal of Photoenergy* **2013**, *2013*, 1-9.

[20] M. Carnie, D. Bryant, T. Watson, D. Worsley, *International Journal of Photoenergy* **2012**, *2012*, 1-8.

[21] S. Mastroianni, A. Lanuti, S. Penna, A. Reale, T. M. Brown, A. Di Carlo, F. Decker, *Chemphyschem : a European journal of chemical physics and physical chemistry* **2012**, *13*, 2925-2936.

[22] C.-H. Lee, K.-M. Lee, Y.-L. Tung, J.-M. Wu, *Journal of The Electrochemical Society* **2012**, *159*, B430-B433.

[23] K. Zhu, S.-R. Jang, A. J. Frank, *Energy & Environmental Science* **2012**, *5*, 9492-9495.

[24] M. I. Asghar, K. Miettunen, J. Halme, P. Vahermaa, M. Toivola, K. Aitola, P. Lund, *Energy & Environmental Science* **2010**, *3*, 418-426.

[25] S. Zhang, X. Yang, Y. Numata, L. Han, *Energy & Environmental Science* **2013**, *6*, 1443-1464.

[26] (a) D. Ciobanu, I. Visa, A. Duta, *Energy Procedia* **2014**, *48*, 707-714; (b) K. Miettunen, J. Etula, T. Saukkonen, S. Jouttijärvi, J. Halme, J. Romu, P. Lund, *Progress in Photovoltaics: Research and Applications* **2014**, DOI: 10.1002/pip.2534.

[27] A. G. Kontos, T. Stergiopoulos, V. Likodimos, D. Milliken, H. Desilvesto, G. Tulloch, P. Falaras, *The Journal of Physical Chemistry C* **2013**, *117*, 8636-8646.

[28] (a) J. Wu, Z. Lan, J. Lin, M. Huang, S. Hao, L. Fang, *Electrochimica Acta* **2007**, *52*, 7128-7135; (b) S. R. Kim, M. K. Parvez, I. In, H. Y. Lee, J. M. Park, *Electrochimica Acta* **2009**, *54*, 6306-6311; (c) S. J. Lim, Y. S. Kang, D.-W. Kim, *Electrochemistry Communications* **2010**, *12*, 1037-1040; (d) O.

Winther-Jensen, V. Armel, M. Forsyth, D. R. Macfarlane, *Macromol. Rapid. Commun.* **2010**, *31*, 479-483.

[29] G.R.A.Kumara, S.Kaneko, M.Okura, K.Tennakone, *Langmuir* **2002**, *18*, 10493-10495.

[30] (a) J. Hagen, W. Schaffrath, P. Otschik, R. Fink, A. Bacher, H.-W. Schmidt, D. Haarer, *Synthetic Metals* **1997**, *89*, 215-220; (b) K. Murakoshi, R. Kogure, Y. Wada, S. Yanagida, *Solar Energy Materials and Solar Cells* **1998**, *55*, 113-115.

[31] A. Yella, H. W. Lee, H. N. Tsao, C. Yi, A. K. Chandiran, M. K. Nazeeruddin, E. W. Diau, C. Y. Yeh, S. M. Zakeeruddin, M. Grätzel, *Science* **2011**, *334*, 629-634.

[32] C. Zhang, Y. Huang, S. Chen, H. Tian, L. e. Mo, L. Hu, Z. Huo, F. Kong, Y. Ma, S. Dai, *The Journal of Physical Chemistry C* **2012**, *116*, 19807-19813.

[33] G. Xue, Y. Guo, T. Yu, J. Guan, X. Yu, J. Zhang, J. Liu, Z. Zou, *Int. J. Electrochem. Sci.* **2012**, *7*, 1496-1511.

[34] (a) S. Sarker, H. W. Seo, D. M. Kim, *Chemical Physics Letters* **2013**, *585*, 193-197; (b) A. Asghar, M. Emziane, H. K. Pak, S. Y.

Oh, *Solar Energy Materials and Solar Cells* **2014**, *128*, 335-342.

[35] U. Opara Krašovec, M. Bokalič, M. Topič, *Solar Energy Materials and Solar Cells* **2013**, *117*, 67-72.

[36] J. Kalowekamo, E. Baker, *Solar Energy* **2009**, *83*, 1224-1231.

[37] (a) B. E. Hardin, H. J. Snaith, M. D. McGehee, *Nature Photonics* **2012**, *6*, 162-169; (b) A. Hinsch, W. Veurman, H. Brandt, K. F. Jensen, S. Mastroianni, *Chemphyschem : a European journal of chemical physics and physical chemistry* **2014**, *15*, 1076-1087.

[38] (a) H.-S. Lee, C.-H. Han, Y.-M. Sung, S. S. Sekhon, K.-J. Kim, *Current Applied Physics* **2011**, *11*, S158-S162; (b) S. J. Lim, Y. S. Kang, D.-W. Kim, *Electrochimica Acta* **2011**, *56*, 2031-2035.

[39] L. Kavan, M. Grätzel, *Electrochimica Acta* **1989**, *34*, 1327-1334.

[40] D. M. Han, K.-W. Ko, C.-H. Han, Y. S. Kim, *Journal of Materials Chemistry A* **2013**, *1*, 8529-8533.

[41] T. Katakabe, R. Kawano, M. Watanabe, *Electrochemical and Solid-State Letters* **2007**, *10*, F23-F25.

[42] S. P. Mohanty, P. Bhargava, *Journal of Power Sources* **2012**, *218*,

174-180.

[43] (a) R. Kawano, M. Watanabe, *Chemical Communications* **2003**, 330-331; (b) R. Kawano, M. Watanabe, *Chem. Commun.* **2005**, 2107-2109.

[44] H. J. Snaith, A. Petrozza, S. Ito, H. Miura, M. Grätzel, *Advanced Functional Materials* **2009**, *19*, 1810-1818.

[45] A. Hauch, A. Georg, *Electrochimica Acta* **2001**, *46*, 3457-3466.

[46] J. Wang, J. Wu, H. Li, *Material Matters* **2012**, *7*, 2-6.

[47] Q. L. Wu, N. Subramanian, S. E. Rankin, *Langmuir* **2011**, *27*, 9557-9566.

[48] B. Wang, S. Chang, L. T. Lee, S. Zheng, K. Y. Wong, Q. Li, X. Xiao, T. Chen, *ACS Appl. Mater. Interfaces* **2013**, *5*, 8289-8293.

[49] (a) J. Liu, H. Yang, W. Tan, X. Zhou, Y. Lin, *Electrochimica Acta* **2010**, *56*, 396-400; (b) Y. Duan, N. Fu, Q. Liu, Y. Fang, X. Zhou, J. Zhang, Y. Lin, *Journal of Physical Chemistry C* **2012**, *116*, 8888-8893.

[50] T.-Y. Cho, C.-W. Han, Y. Jun, S.-G. Yoon, *Scientific reports*

2013, *3*, 1496-1503.

[51] D. M. Han, K.-W. Ko, C.-H. Han, Y. S. Kim, *RSC Advances* **2014**, *4*, 28133-28140.

[52] (a) K.Wagner, M.J.Griffith, M.James, A.J.Mozer, P.Wagner, G.Triani, D.L.Officer, G.G.Wallace, *Journal of Physical Chemistry C* **2011**, *115*, 317-326; (b) C. Chen, X. Yang, M. Cheng, F. Zhang, L. Sun, *ChemSusChem* **2013**, *6*, 1270-1275.

[53] (a) S. Mastroianni, I. Asghar, K. Miettunen, J. Halme, A. Lanuti, T. M. Brown, P. Lund, *Phys. Chem. Chem. Phys.* **2014**, *16*, 6092-6100; (b) X. Y. Huang, J. X. Wang, D. C. Yu, S. Ye, Q. Y. Zhang, X. W. Sun, *Journal of Applied Physics* **2011**, *109*, 113526.

[54] (a) J. Dewalque, N. D. Nguyen, P. Colson, N. Krins, R. Cloots, C. Henrist, *Electrochimica Acta* **2014**, *115*, 478-486; (b) M. Giustini, D. Angelone, M. Parente, D. Dini, F. Decker, A. Lanuti, A. Reale, T. Brown, A. di Carlo, *Journal of Applied Electrochemistry* **2013**, *43*, 209-215; (c) N. Kato, Y. Takeda, K. Higuchi, A. Takeichi, E. Sudo, H. Tanaka, T. Motohiro, T. Sano, T. Toyoda, *Solar Energy Materials and Solar Cells* **2009**, *93*, 893-897; (d) H. Pettersson, T. Gruszecki, *Solar Energy Materials and Solar Cells* **2001**, *70*,

203-212.

[55] M. Carnie, T. Watson, D. Worsley, *International Journal of Photoenergy* **2012**, *2012*, 1-9.

[56] M. Berginc, U. O. Krašovec, M. Topič, *Solar Energy Materials and Solar Cells* **2014**, *120*, 491-499.

[57] D. V. Pogozhev, M. J. Bezdek, P. A. Schauer, C. P. Berlinguette, *Inorg. Chem.* **2013**, *52*, 3001-3006.

[58] (a) E. Klampaftis, D. Ross, K. R. McIntosh, B. S. Richards, *Solar Energy Materials and Solar Cells* **2009**, *93*, 1182-1194; (b) C. K. Hong, H.-S. Ko, E.-M. Han, J.-J. Yun, K.-H. Park, *Nanoscale Research Letters* **2013**, *8*, 219-225; (c) X. Huang, S. Han, W. Huang, X. Liu, *Chem. Soc. Rev.* **2013**, *42*, 173-201; (d) Y.-J. Lin, C.-C. Chang, S.-J. Cherng, J.-W. Chen, C.-M. Chen, *Progress in Photovoltaics: Research and Applications* **2013**, DOI: 10.1002/pip.2407.

[59] M. Zahedifar, Z. Chamanzadeh, S. M. Hosseinpoor Mashkani, *Journal of Luminescence* **2013**, *135*, 66-73.

[60] (a) J. Xu, H. Zhang, Q. Xiong, G. Liang, L. Wang, X. Shen, L.

Liu, W. Xu, *Journal of Physics: Conference Series* **2011**, *276*, 012195; (b) Z. Hosseini, W. K. Huang, C. M. Tsai, T. M. Chen, N. Taghavinia, E. W. Diau, *ACS applied materials & interfaces* **2013**, *5*, 5397-5402.

[61] V. Badescu, A. De Vos, *Journal of Applied Physics* **2007**, *102*, 073102.

[62] J. Liu, Q. Yao, Y. Li, *Applied Physics Letters* **2006**, *88*, 173119.

[63] (a) S.R.Patil, S.B.Patwari, *Journal of Luminescence* **1999**, *82*, 115-119; (b) O. Divya, A. K. Mishra, *Analytica chimica acta* **2008**, *630*, 47-56.

[64] F. De Angelis, S. Fantacci, E. Mosconi, M. K. Nazeeruddin, M. Grätzel, *The Journal of Physical Chemistry C* **2011**, *115*, 8825-8831.

초 록

염료감응형 태양전지의 안정성을 개선할 수 있는 새로운 개념의 제조 방법 (double layer gel-type electrolyte and dimeric complex forming spectrum conversion layer)을 개발하였다. 또한, 계층형 구조 형성공정을 준고체 전해질 염료감응형 태양전지에 최적화하였다. (micro-crater structure of photo-anode)

안정성을 개선하기 위하여는 염료와 전해질, 특히 야외에서 사용 시에는 자외선차단필터의 선택이 가장 중요하다. 이 가운데, 염료는 높은 광전변환 효율과 안정성이 검증된 루테늄 계열 (N719)이 널리 사용되고 있으며 신규 염료에 대한 연구가 진행되고 있다. 하지만, 전해질과 자외선차단필터에 있어서는 광전변환 효율과 안정성이 양립하지 못하는 모순관계가 있어왔다.

안정적인 자외선 경화 고분자 겔 전해질의 광전변환 효율을 개선하기 위하여 상기의 전해질과 상대전극 사이에 나노 겔 전해질 층을 도입하였다. 그 결과로 형성된 이중층 겔 타입 전해질은 두께가 증가했음에도 불구하고 교환반응에 의한 전하 확산효과가 커져서 낮은 전하 전달 저항을 보여주었다.

준고체 전해질의 사용에서 중요한 점은 TiO_2 나노입자

필름과 전해질 사이의 접촉저항을 낮추는 것이다. 전해질이 빠르고 완전하게 침투할 수 있도록 고온에서 증발하는 아세틸렌블랙을 사용하여 미세 분화구 모양의 구조를 형성하였다. 이 형상을 가진 TiO_2 나노입자 필름은 별도의 광확산 필름층을 사용하지 않고도 뛰어난 광확산 효과를 보여주었다.

TiO_2 나노입자 필름은 광음극의 필수적인 구조를 제공하지만 야외에서 자외선을 흡수하여 염료과 전해질을 분해하고 안정성을 저해한다. 유해한 자외선이 TiO_2 필름에 도달하기 전에 장파장으로 변환하기 위하여, 광음극 위에 파장변환 층을 추가로 도입하였다. 유사한 구조의 두 개의 파장변환 소재는 높은 농도에서 여기자 복합체를 형성하고 스토크 변환을 증가시켰다.

상기의 세 가지 안정성 개선 방법은 예상치 못한 환경의 영향을 제거하기 위하여 전통적인 염료감응형 태양전지에서 개발되었으나, 여러 가지 종류와 형태의 차세대 태양전지에도 유용한 새로운 기술이다.

주 요 어 : 염료감응형 태양전지, 안정성, 겔타입 전해질, 계층형 구조, 파장변환 물질

학 번 : 2010-30738